National Oceanography Centre, Southampton

Internal Document No. 14

Airflow distortion at anemometer sites on the OWS *Polarfront*

B I Moat & M J Yelland

2009

National Oceanography Centre, Southampton
University of Southampton, Waterfront Campus
European Way
Southampton
Hants SO14 3ZH
UK

Author contact details
Tel: +44 (0)23 8059 7739
Email: bim@noc.soton.ac.uk

DOCUMENT DATA SHEET

AUTHOR
MOAT, B I & YELLAND, M J

PUBLICATION DATE 2009

TITLE
Airflow distortion of anemometer sites on the OWS *Polarfront*.

REFERENCE
Southampton, UK: National Oceanography Centre, Southampton, 35pp.
(National Oceanography Centre Southampton Internal Document, No. 14)
(Unpublished manuscript)

ABSTRACT

Accurate wind speed measurements from anemometers on research ships are required to obtain high quality air-sea flux measurements. However, the measurements can be biased by the distortion of the airflow over the ship, i.e. the wind speed can either be accelerated or decelerated by the presence of the ship and the flow of air can be displaced vertically over the ship's superstructure. The computational fluid dynamics software VECTIS was used to numerically simulate the airflow over the Ocean Weather Ship Polarfront. The airflow distortion at six anemometer sites has been quantified for a wind speed of 10 ms-1 blowing a) directly over the bows of the ship and b) over the ship's starboard beam. The wind speed errors ranged from decelerations of about 1 % for an airflow directly over the bow to accelerations of 10 % for the beam-on flow.

KEYWORDS

ISSUING ORGANISATION

National Oceanography Centre, Southampton
University of Southampton, Waterfront Campus
European Way
Southampton SO14 3ZH
UK

AIRFLOW DISTORTION AT ANEMOMETER SITES ON THE OCEAN WEATHER SHIP *POLARFRONT*

CONTENTS

1. Introduction **1**

2. Description of the CFD modelling **1**

3. Anemometer positions **3**

4. wind speed error calculation **3**

5. *Polarfront* "hove-to" (model run 3.10/4) **4**

5.1 Introduction 4

5.2 The free stream flow 4

5.3 The vertical displacement of the flow 5

5.4 The wind speed error 6

6. *Polarfront* "beam-on" (model run 3.10/3) **8**

6.1 Introduction 8

6.2 The free stream flow 9

6.3 The vertical displacement of the flow 9

6.4 The wind speed error 10

7. Summary **12**

Acknowledgements **15**

References **15**

Figures **16**

AIRFLOW DISTORTION AT ANEMOMETER SITES ON THE OCEAN WEATHER SHIP *POLARFRONT*

B. I. Moat and M. J. Yelland

February 2009

1. INTRODUCTION

Wind speed measurements from ship-based anemometers are biased by the distortion of the airflow by the ship's hull and superstructure. For example, previous computational fluid dynamics (CFD) modelling has shown that well-exposed anemometers located on the foremasts of research ships can experience a flow distortion of up to 8 % (Yelland et al., 2002). This report documents the results of the CFD modelling of the OWS *Polarfront* at two relative wind directions and presents the correction factors, which need to be applied to the wind speed data.

The *Polarfront* and its predecessors have occupied station MIKE (66°N 2°E) in the Norweign Sea continuously for nearly 60 years, only coming into port for 8 hours once a day. The *Polarfront* is operated in two modes; 1) during light and moderate conditions the ship drifts beam-on, with the wind blowing onto the starboard side, 2) in high winds speeds and/or large seas the ship is 'hove-to' with the wind blowing directly over the bow. From September 2006 to September 2012 the National Oceanography Centre supplemented the Norwegian Meteorological Institute (DNMI) meteorological instrumentation with the AutoFlux system (Yelland et al., 2009). The anemometers were situated in a well exposed location on the ship's foremast. In order to proceed with the data analysis it was necessary first to quantify the effects of the flow distortion and then to correct the measurements obtained from the ship.

The Computational Fluid Dynamics package VECTIS (Ricardo, 2005) was used to simulate the flow of air around the *Polarfront*. The VECTIS code is described in Section 2 and the anemometer locations are described in Section 3. Compared to a freestream (undisturbed) flow, the airflow at an anemometer site may have been accelerated (or decelerated) and displaced upwards. The method used to calculate the percentage error at an anemometer site is detailed in Section 4. Two model runs were performed; run 3.10/4 simulated a flow of air directly over the bows of the ship (Section 5), and run 3.10/3 simulated a flow 100 degrees aft of the bow onto the starboard beam of the ship (Section 6). The wind speed errors are calculated for the six anemometer sites for both model runs. The results are summarised in Section 7.

2. DESCRIPTION OF THE CFD MODELLING

VECTIS is a commercial three-dimensional Reynolds Averaged Navier-Stokes solver, which has been used successfully since 1994 to model the airflow over many research ships (Yelland et al. 1998; 2002). The VECTIS models only reproduce the steady state mean flow characteristics, and do not simulate the turbulence structure. The standard $k \sim \varepsilon$

(Launder and Spalding, 1972) turbulence closure model was used to parameterise the turbulence. Except when the anemometer is in the wake of an upstream obstacle, VECTIS simulations of the airflow over detailed ship models are accurate to within 2 % (Yelland et al. 2002) for well-exposed anemometer locations on research ships.

A numerical representation of the full-scale 3-dimensional ship geometry was created by digitizing the 2-dimensional ships plans using the digitizing software DIDGER (DIDGER, 2008). Over a period of 2 weeks the software package FEMGEN (Femsys, 1992) was used to convert the digitized 2-dimensional plans into the 3-dimensional geometry required by the VECTIS software. The numerical representation of the geometry was very detailed (Figure 1) and reproduced the actual geometry to within 0.1 m. The general ship dimensions are 54 m in overall length and 10 m in breadth. The *Polarfront* floats 0.65 m lower in the water when compared to the plans. This was accounted for in the geometry. A computational domain was defined around the geometry with the ship in the centre. The width of the domain increased with the ship's orientation to the flow to prevent spurious increases in wind speed created by the blockage of the ship in the domain. For flows directly over the bow (head to wind) the domain size was 600 m in length, 300 m wide and 150 m high. For the second simulation with a relative wind directions of 100° off the bow the domain width increased to 1400 m. In general, the ratio of the frontal area of the ship to the area of the inlet gave a blockage by the ship of less than 1 %.

The number of computational cells within the domain increased from 1.5 million for the flow directly over the bow to 3.2 million at a relative wind direction of 100°. The time taken for the solutions to converge was about 10 days using a 2.4 GHz Opteron processor on a Linux workstation. This fast convergence time was obtained using the steady-state rather than the time-marching solver (Moat and Yelland, 2006). The cell sizes varied throughout the computational domain with high-resolution cells in the vicinity of the foremast (cells of 0.08 m) and much lower resolution cells in areas well away from the ship where the flow did not vary very rapidly.

The vertical profile of the wind speed specified at the domain inlet was specified as a fully logarithmic boundary layer profile, with a 10 m neutral wind speed, U_{10n}, of 10 m/s;

$$U_{10n} = \frac{u_*}{k_v} \ln\left(\frac{10}{z_0}\right) \qquad (1)$$

where k_v is the von Kármán constant (value 0.4), z_0 is the roughness length (value 1.16×10^{-4} m) and u_* is the friction velocity calculated from the Smith, (1980) drag coefficient relationship. The domain floor was allocated a small roughness length (order 10^{-4} m) in order to maintain the profile downwind of the inlet. All results presented in this report were obtained by comparing the wind speed at a particular anemometer position with the freestream wind speed profile well abeam (more than 100 m) of the anemometer position to arrive at a percentage wind speed bias for that position.

3. ANEMOMETER POSITIONS

The locations of the three anemometer sites are shown in Figure 1 and 2. Before September 2006 DMNI had two Gill WindObserver anemometers located on the foremast. One wind master was removed to make way for the R3 sonic anemometer used by the AuftoFlux system. In addition, during 2008 the height of the R3 sonic anemometer was changed slightly due to different mounting configurations. Where necessary the dates of the changes are indicated in the following table. In the VECTIS model co-ordinates system, the anemometer positions are;

	Anemometer	X, along (m)	Y, across (m)	Z, above (m)
0 degrees Head to wind	R3 anemometer (pre-Jan 2008)	19.62	-0.83	15.5
	R3 anemometer (Jan-April 2008)	19.62	-0.83	15.57
	R3 anemometer (post-April 2008)	19.62	-0.83	15.27
	DNMI WindObserver	19.62	-0.33	15.26
	DNMI WindObserver (pre September 2006)	19.62	-0.83	15.26
	DNMI propeller anemometer	19.61	0.83	15.25
100 degrees from bow	R3 anemometer (pre-Jan 2008)	-2.59	19.46	15.5
	R3 anemometer (Jan-April 2008)	-2.59	19.46	15.57
	R3 anemometer (post-April 2008)	-2.59	19.46	15.27
	DNMI WindObserver	-3.08	19.38	15.26
	DNMI WindObserver (pre September 2006)	-2.59	19.46	15.26
	DNMI propeller anemometer	-4.22	19.17	15.25

Table 1 Anemometers positions in the VECTIS co-ordinate system. The z value is the height of the anemometer above the design waterline of the ship. A schematic of the locations are shown in Figures 2.

4. WIND SPEED ERROR CALCULATION

The flow at the instrument site can suffer from server distortion and large gradients in the velocity field. Additionally it is not always possible to define the mesh so that the instruments are at the exact centers of the computational cells (see Moat et al., 1996). Therefore the velocity at an instrument site was obtained from an average of three values

estimated from lines of data extracted in three directions. The percentage wind speed error is given by:

$$\%Error = \left(\frac{Average\ velocity}{Free\ stream\ velocity} - 1 \right) \times 100 \qquad (2)$$

with a positive error indicating an acceleration of the flow. The percentage error is calculated using the free stream flow at the height of the anemometer and at the height the airflow originated, i.e. taking into account the vertical displacement of the airflow.

5. *POLARFRONT* "HOVE-TO" (MODEL RUN 3.10/4)

5.1 Introduction

This section describes the modelling of the airflow over the *Polarfront* at 0º to the flow, i.e. for a wind blowing directly on to the bows of the ship ("mode 2", Section 1). A complete description of the procedures used can be found in Moat et. al. (1996). While the computational solver was running, the residuals were monitored and with the exception of viscous dissipation (TE) were less than 10^{-6} after 24,592 iterations (Figure 3). TE with residuals of the order of 10^{-5} does not affect the mean flow in the computational domain. A post-processing file was written for the extraction of data throughout the computational volume. These data were first used to check that the flow at the sides and ends of the tunnel was undisturbed by the presence of the ship and could therefore be used to estimate the free stream flow (Section 5.2). The vertical displacement of the flow at the anemometer site was quantified (Section 5.3). The absolute wind speed bias was calculated as well as the wind speed bias accounting for the vertical displacement of the air (Section 4.4).

5.2 The free stream flow

Figure 4 shows horizontal lines of velocity data which were extracted along the length of the tunnel at heights of 10, 20,30 and 50 m, on a plane at y = 140 m, i.e. towards the side of the tunnel. The middle section of the tunnel only is shown in more detail in Figure 5, which displays velocity data directly abeam of the ship (-50 m < x < 50 m). These figures show that the velocity at a particular height changed little (about 0.05 m/s or less) along the length of the tunnel, and that the presence of the ship in the centre of the tunnel was not causing any significant blockage to the flow at the sides of the tunnel. This is confirmed in Figures 6 and 7. Figure 6 shows the vertical profiles of the wind speed at the tunnel "inlet" (x = 275 m) and "outlet" (x = -275 m), and Figure 8 shows the difference between these two profiles. Below about 5 m the relatively large difference (1 m/s) between the two profiles is due to the steep wind speed gradient exaggerating the effect of a small change in the shape of the profile. Above 5 m, the difference between the profiles is less than 0.05 m/s on average. These figures show that the shape of the wind speed profile changes slightly along the tunnel. Because of this small change, the free stream velocities are estimated using the vertical

profiles of velocity 100 m abeam of the anemometer site, rather than the profiles at the tunnel inlet or outlet.

5.3 The vertical displacement of the flow

To calculate the vertical displacement of the flow reaching the anemometer a streamline is traced from the anemometer site upstream to the anemometer location. Tables 1 to 6 give the coordinates of; "Z_{anemom}" the foremast anemometer site, and the position of the start of the streamline "Z_{origin}". It can be seen that the streamline reaching the R3 sonic anemometer site (pre-January 2008) is displaced vertically by 1.25 m.

location	x (m)	y (m)	z (m)
Z_{anemom}	19.616	-0.83	15.5
Z_{origin}	278	-0.83	14.252
$Z_{anemom} - Z_{origin}$	-258.4	0	$\mathbf{\Delta z}$ = 1.25

Table 1 The vertical displacement, Δz, of the flow to the R3 anemometer (pre-January 2008)

location	x (m)	y (m)	z (m)
Z_{anemom}	19.616	-0.83	15.565
$Z_{upstream}$	278	-0.83	14.315
$Z_{anemom} - Z_{origin}$	-258.4	0	$\mathbf{\Delta z}$ = 1.25

Table 2 The vertical displacement, $\Delta\mathbf{z}$, of the flow to the R3 anemometer (Jan-April 2008).

location	x (m)	y (m)	z (m)
Z_{anemom}	19.616	-0.83	15.27
$Z_{upstream}$	278	-0.83	13.99
$Z_{anemom} - Z_{upstream}$	-258.4	0	$\mathbf{\Delta z}$ = 1.28

Table 3 The vertical displacement, $\Delta\mathbf{z}$, of the flow to the R3 anemometer (post-April 2008).

location	x (m)	y (m)	z (m)
Z_{anemom}	19.616	-0.33	15.26
$Z_{upstream}$	278	-0.33	13.98
$Z_{anemom} - Z_{origin}$	-258.4	0	$\mathbf{\Delta z}$ = 1.28

Table 4 The vertical displacement, $\Delta\mathbf{z}$, of the flow to the DNMI WindObserver

location	x (m)	y (m)	z (m)
Z_{anemom}	19.616	-0.83	15.26
$Z_{upstream}$	278	-0.83	13.98
$Z_{anemom} - Z_{upstream}$	-258.4	0	$\mathbf{\Delta z}$ = 1.28

Table 5 The vertical displacement, $\Delta\mathbf{z}$, of the flow to the DNMI WindObserver (pre September 2006)

location	x (m)	y (m)	z (m)
Z_{anemom}	19.611	0.83	15.25
$Z_{upstream}$	278	0.83	13.96
Z_{anemom}-$Z_{upstream}$	-258.4	0	$\mathbf{\Delta z}$ = 1.29

Table 6 The vertical displacement, $\Delta\mathbf{z}$, of the flow to the DNMI propeller anemometer

These estimates of the vertical displacement were used to obtain the free stream velocities for the anemometer sites. The air parcel reaching the anemometer will have originated at a height of (anemometer height-$\mathbf{\Delta z}$), and the free stream velocity is obtained at that height on the free stream profile. For example, Figure 8 shows the free stream profile directly abeam of the foremast anemometer (x = 19.616m, 0 < y < 150m, z = 145m), which gives a free stream velocity of 10.251 m/s at a height of 13.99 m.

5.4 The wind speed error

Figures 9 to 14 show the lines of velocity data through the six anemometer locations for a wind directly over the bow. The percentage wind speed errors for all anemometer sites are summarized in Table 7. A positive error indicates an acceleration of the flow. Figures 9 to 14 are also used to estimate the gradient of the velocity of the flow in all three directions. These rate of change of velocity provide an indication of the accuracy of the velocity error estimate and also demonstrate whether a site is suitable for obtaining reliable wind speed measurements. The rates of change for the anemometer sites are given in terms of change per cell and per meter in Table 8 and are small. In general, the effects of flow distortion at all the anemometer sites are small, with the flow being displaced vertically by 1.3 m and decelerated by about 1 % or less.

Anemometer site	Velocity from each direction (m/s)	Average velocity (m/s)	Free stream velocity (m/s)	% Error	Angle from horizontal (degrees)
R3 pre-January 2008	10.237 (x)		10.346	**-1.05**	
	10.238 (y)	10.237			5.0
	10.237 (z)		10.268 (Δz)	-0.3 (Δz)	
R3 January to April 2008	10.238 (x)		10.345	**-1.02**	
	10.239 (y)	10.239			4.9
	10.239 (z)		10.272 (Δz)	-0.32 (Δz)	
R3 post-April 2008	10.237 (x)		10.332	**-0.93**	
	10.233 (y)	10.236			5.0
	10.237 (z)		10.251 (Δz)	-0.15 (Δz)	
DNMI WindObserver	10.179 (x)		10.331	**-1.47**	
	10.180 (y)	10.179			5.2
	10.179 (z)		10.250 (Δz)	-0.69 (Δz)	
DNMI WindObserver Pre Sept 2008	10.237(x)		10.332	**-0.91**	
	10.238 (y)	10.238			5.3
	10.238 (z)		10.251 (Δz)	-0.13 (Δz)	
DNMI propeller	10.234 (x)		10.333	**-0.95**	
	10.237 (y)	10.235			5.3
	10.234 (z)		10.252 (Δz)	-0.16 (Δz)	

Table 7 Percentage absolute velocity error (bold) and velocity error taking into account the vertical displacement of the air at the anemometer sites (indicated by Δz). The angle of the airflow (tilt) from the horizontal at the anemometer sites are included. Results are from a flow directly over the bow.

Anemometer site	Velocity data line	Rate of change of velocity per metre (ms^{-1}/m)	Rate of change of velocity per cell (ms^{-1}/cell)
R3 pre-January 2008	along (x)	-0.140	-0.006
	across (y)	0.065	-0.004
	up (z)	0.044	0.001
R3 January to April 2008	along (x)	-0.13	-0.006
	across (y)	-0.065	-0.003
	up (z)	0.025	0.001
R3 post-April 2008	along (x)	-0.155	-0.008
	across (y)	-0.06	-0.009
	up (z)	0.015	0.001
DNMI WindObserver	along (x)	0.005	0.005
	across (y)	-0.025	-0.01
	up (z)	0.02	-0.001
DNMI WindObserver Pre Sept 2008	along (x)	-0.16	-0.008
	across (y)	-0.06	-0.009
	up (z)	0.005	-0.001
DNMI propeller	along (x)	-0.16	-0.009
	across (y)	0.050	0.008
	up (z)	0.022	0.012

Table 8 Rate of change of velocity close to the anemometer sites. Results are from a flow directly over the bow.

6. *POLARFRONT* "BEAM-ON" (MODEL RUN 3.10/3)

6.1 Introduction

This section describes the modelling of the airflow over the *Polarfront* at 100º from the bow i.e. for a wind blowing on to the starboard beam of the ship ("mode 1", Section 1). A complete description of the procedures used can be found in Moat et. al. (1996). While the computational solver was running, the residuals were monitored and with the exception of viscous dissipation (TE) were less than 10^{-6} after 16,000 iterations (Figure 15). TE with residuals of the order of 10^{-5} does not affect the mean flow in the computational domain. A post-processing file was written for the extraction of data throughout the computational volume. These data were first used to check that the flow at the sides and ends of the tunnel was undisturbed by the presence of the ship and could therefore be used to estimate the free stream flow (Section 6.2). The vertical displacement of the flow at the anemometer site was quantified (Section 6.3). The absolute wind speed bias was calculated as well as the wind speed bias accounting for the vertical displacement of the air (Section 6.4).

6.2 The free stream flow

Figure 16 shows horizontal lines of velocity data which were extracted along the length of the tunnel at heights of 10, 30 and 50 m, on a plane at y = 675 m, i.e. towards the side of the tunnel. The middle section of the tunnel only is shown in more detail in Figure 17, which displays velocity data directly abeam of the ship (-50 m < x < 50m). These figures show that the velocity at a particular height changed little (about 0.05 m/s or less) along the length of the tunnel, and that the presence of the ship in the centre of the tunnel was not causing any significant blockage to the flow at the sides of the tunnel. This is confirmed in Figures18 and 19. Figure 18 shows the vertical profiles of the wind speed at the tunnel "inlet" (x = 275 m) and "outlet" (x = -275 m), and Figure 19 shows the difference between these two profiles. Below about 5 m the relatively large difference (1 m/s) between the two profiles is due to the steep wind speed gradient exaggerating the effect of a small change in the shape of the profile. Above 5 m, the difference between the profiles is less than 0.05 m/s on average. These figures show that the shape of the wind speed profile changes slightly along the tunnel. Because of this small change, the free stream velocities are estimated using the vertical profiles of velocity 675 m abeam of the anemometer site, rather than the profiles at the tunnel inlet or outlet.

6.3 The vertical displacement of the flow

To calculate the vertical displacement of the flow reaching the anemometer a streamline is traced from the anemometer site upstream to the anemometer location. Tables 9 to 15 give the coordinates of; "Z_{anemom}" the foremast anemometer site, and the position of the start of the streamline "Z_{origin}". It can be seen that the streamline reaching the R3 sonic anemometer site (pre-January 2008) is displaced vertically by 4.36 m.

location	x (m)	y (m)	z (m)
Z_{anemom}	-2.59	19.46	15.5
Z_{origin}	275	19.46	11.14
Z_{anemom} -Z_{origin}	-277.59	0	$\mathbf{\Delta z}$ = 4.36

Table 9 The vertical displacement, Δz, of the flow to the R3 anemometer (pre-January 2008)

location	x (m)	y (m)	z (m)
Z_{anemom}	-2.59	19.46	15.57
$Z_{upstream}$	275	19.46	11.22
Z_{anemom} -Z_{origin}	-277.59	0	$\mathbf{\Delta z}$ = 4.35

Table 10 The vertical displacement, $\Delta \mathbf{z}$, of the flow to the R3 anemometer (Jan-April 2008).

location	x (m)	y (m)	z (m)
Z_{anemom}	-2.59	19.46	15.27
$Z_{upstream}$	275	-0.83	10.87
Z_{anemom}-$Z_{upstream}$	-277.59	0	$\mathbf{\Delta z}$ = 4.40

Table 12 The vertical displacement, $\Delta\mathbf{z}$, of the flow to the R3 anemometer (post-April 2008).

location	x (m)	y (m)	z (m)
Z_{anemom}	-3.08	19.38	15.26
$Z_{upstream}$	275	19.38	10.71
Z_{anemom} -Z_{origin}	-278.08	0	$\mathbf{\Delta z}$ = 4.55

Table 13 The vertical displacement, $\Delta\mathbf{z}$, of the flow to the DNMI WindObserver

location	x (m)	y (m)	z (m)
Z_{anemom}	-2.59	19.46	15.26
$Z_{upstream}$	275	19.46	10.87
Z_{anemom}-$Z_{upstream}$	-258.4	0	$\mathbf{\Delta z}$ = 4.39

Table 14 The vertical displacement, $\Delta\mathbf{z}$, of the flow to the DNMI WindObserver (pre September 2006).

location	x (m)	y (m)	z (m)
Z_{anemom}	-4.22	19.17	15.25
$Z_{upstream}$	276	19.17	10.38
Z_{anemom}-$Z_{upstream}$	-280.22	0	$\mathbf{\Delta z}$ = 4.87

Table 15 The vertical displacement, $\Delta\mathbf{z}$, of the flow to the DNMI propeller anemometer

These estimates of the vertical displacement were used to obtain the free stream velocities for the anemometer sites. The air parcel reaching the anemometer will have originated at a height of (anemometer height-$\mathbf{\Delta z}$), and the free stream velocity is obtained at that height on the free stream profile. The variation of the vertical displacement of the flow to the R3 anemometer site is shown in Figure 20. The displacement begins about 7 seconds upstream of the anemometers.

6.4 The wind speed error

Figures 21 to 26 show the lines of velocity data through the six anemometer locations for a wind directly over the bow. The percentage wind speed errors for all anemometer sites are summarized in Table 16. A positive error indicates an acceleration of the flow. Figures 21 to 26 are also used to estimate the gradient of the velocity of the flow in all three directions. These rates of change of velocity provide an indication of the accuracy of the velocity error estimate and also demonstrate whether a site is suitable for obtaining reliable wind speed measurements. The rates of change for the anemometer sites are given in terms of change per

cell and per meter in Table 17 and are small. In general the effects of flow distortion at all the anemometer sites are moderate with the flow being displaced vertically by about 4.5 m and accelerated by 8 to 11 %.

Anemometer site	Velocity from each direction (m/s)	Average velocity (m/s)	Free stream velocity (m/s)	% Error	Tilt from horizontal (degrees)
R3 pre-January 2008	10.837 (x)		10.337	**4.80**	
	10.838 (y)	10.838			10.2
	10.838 (z)		10.046 (Δz)	7.88 (Δz)	
R3 January to April 2008	10.834 (x)		10.341	**4.78**	
	10.836 (y)	10.835			10.1
	10.835 (z)		10.052 (Δz)	7.79 (Δz)	
R3 post-April 2008	10.846 (x)		10.324	**5.07**	
	10.848 (y)	10.847			10.5
	10.847 (z)		10.027	8.18 (Δz)	
DNMI WindObserver	11.025 (x)		10.321	**6.83**	
	11.027 (y)	11.026			9.9
	11.026 (z)		10.012 (Δz)	10.13 (Δz)	
DNMI WindObserver Pre Sept 2008	10.846 (x)		10.322	**5.09**	
	10.848 (y)	10.847			10.5
	10.847 (z)		10.027 (Δz)	8.18 (Δz)	
DNMI propeller	11.100 (x)		10.322	**7.52**	
	11.098 (y)	11.098			8.3
	11.096 (z)		9.992 (Δz)	11.07 (Δz)	

Table 16 Percentage absolute velocity error (bold) and velocity error taking into account the vertical displacement of the air at the anemometer sites (indicated by Δz). The angle of the airflow (tilt) from the horizontal at the anemometer sites are included. Results are from a flow 100° off the starboard bow.

Anemometer site	Velocity data line	Rate of change of velocity per metre (ms^{-1}/m)	Rate of change of velocity per cell (ms^{-1}/cell)
R3 pre-January 2008	along (x)	-0.265	-0.031
	across (y)	0.215	-0.007
	up (z)	-0.025	-0.004
R3 January to April 2008	along (x)	-0.25	-0.031
	across (y)	0.210	0.004
	up (z)	-0.025	-0.003
R3 post-April 2008	along (x)	-0.275	-0.031
	across (y)	0.200	0.004
	up (z)	-0.015	-0.003
DNMI WindObserver	along (x)	-0.215	-0.028
	across (y)	-0.05	-0.012
	up (z)	0.02	-0.005
DNMI WindObserver Pre Sept 2008	along (x)	-0.275	-0.032
	across (y)	0.205	0.004
	up (z)	0.015	-0.003
DNMI propeller	along (x)	0.08	-0.013
	across (y)	1.51	0.002
	up (z)	-0.05	-0.013

Table 17 Rate of change of velocity close to the anemometer sites. Results are from a flow 100° off the starboard bow.

7. SUMMARY

The National Oceanography Centre has supplemented the Norwegian Meteorological Institute (DNMI) meteorological instrumentation on the *Polarfront* with the AutoFlux system (Yelland et al., 2009). Even though the anemometers were situated in a well-exposed location on the ship's foremast they are subject to a biased caused by the presence of the ship distorting the flow of air to the anemometer. The acceleration and vertical displacement of the flow at the anemometer sites have been modeled in three dimensions using computational fluid dynamics (CFD) and are listed in Table 18.

The vertical displacement (Δz) of the flow was used to obtain an effective anemometer height ($z- \Delta z$), and the wind speed error relates the actual flow at the instrument site to the free stream flow at this effective height. The effective height and the correct wind speed relative to this height are required if the data from the anemometer is used to calculate the wind stress via the dissipation method (Yelland *et al.*, 1998). The results for both models and all instrument sites are summarised in Table 18. When the *Polarfront* is hove-to, head to

wind, the airflow at all anemometer sites is slightly decelerated (less than 1 %) and has been displaced upwards by 1.3 m. In contrast, when the ship is beam-on it presents a much larger and more abrupt obstruction to the air flow, causing vertical displacements of the flow of 4 to 5 m at the anemometer sites. In this orientation the flow is accelerated by 5 to 10 % at the anemometers locations. The results differ significantly for the two different wind direction: this is to be expected since the ship presents a larger obstruction when at an angle to the flow than when the flow is over the bows.

The greatest source of error in the results is likely to be in the extraction of the data. The maximum variation of the velocity from one cell to the next in the location of the instruments is 0.012 ms^{-1}/cell and 0.032 ms^{-1}/cell for the bow-on and beam-on flows respectively. For both model runs and all instrument sites, the largest uncertainty in the velocity error is about ±0.3 %.

VECTIS model run	Anemometer site	Velocity at anemometer site (m/s)	Free stream velocity (m/s)	% velocity error at anemometer	Vertical displacement, Δz (m)
Hove-to (3.10/4)	R3 sonic Pre-jan 2008	10.24	10.35 10.27	**-1.1** -0.3 (Δz)	1.3
	R3 sonic Jan-April 2008	10.24	10.35 10.27	**-1.0** -0.3 (Δz)	1.3
	R3 sonic Post-April 2008	10.24	10.33 10.251	**-0.9** -0.2 (Δz)	1.3
	DNMI WindObserver	10.18	10.33 10.25	**-1.5** -0.7 (Δz)	1.3
	DNMI WindObserver Pre-September	10.24	10.33 10.25	-1.5 -0.1 (Δz)	1.3
	DNMI Propeller	10.24	10.33 10.252	-1.0 -0.2 (Δz)	1.3
Beam on (3.10/3)	R3 sonic Pre-jan 2008	10.84	10.34 10.05	**4.8** 7.9 (Δz)	4.4
	R3 sonic Jan-April 2008	10.84	10.34 10.05	**4.8** 7.8 (Δz)	4.4
	R3 sonic Post-April 2008	10.85	10.32 10.03	**5.1** 8.2 (Δz)	4.4
	DNMI WindObserver	11.03	10.32 10.01	**6.8** 10.1 (Δz)	4.4
	DNMI WindObserver Pre-September	10.85	10.32 10.03	**5.1** 8.2 (Δz)	4.4
	DNMI Propeller	11.10	10.32 10.00	**7.5** 11.1 (Δz)	4.9

Table 18 Results from the model simulations of the air flow over the *Polarfront*. The percentage absolute velocity error (bold) and velocity error taking into account the vertical displacement of the air at the anemometer sites (indicated by Δz) are included.

ACKNOWLEDGEMENTS

The HiWSE project was funded by the Natural Environment Research Council, grant number NE/C001826/1. We are grateful to Misje Renderie AS, the ship owners for kindly allowing us to use the *Polarfront*. The officers and crew on the *Polarfront* have been very generous with their help and enthusiasm. Thanks also to Knut Bjorheim of DNMI for permission to use the *Polarfront*. The work was also supported by NOCS funding through the Oceans 2025 program. Lastly thanks to Peter Hunter, NOCS for providing the software to digitize the ship plans.

REFERENCES

Femsys, 1992: FEMGV User Manual, Femsys Ltd., Leicester, United Kingdom, 598 pp.

DIDGER, 2008: available from Golden software http://www.goldensoftware.com/products/didger/didger.shtml

Moat, B. I., M. J. Yelland and J. Hutchings, 1996: Airflow over the R.R.S. Discovery using the Computational Fluid Dynamics package Vectis, SOC Internal Report No. 2, Southampton Oceanography Centre, Southampton, UK. [Available from the National Oceanography Centre, Southampton, UK.].

Moat, B. I. and M. J. Yelland, 2006: Validation of the VECTIS steady-state solver, NOC Internal Document No. 4, National Oceanography Centre, UK. 15pp.[http://eprints.soton.ac.uk/41394/]

Launder, B. E. and D. B. Spalding, 1974: The numerical computation of turbulent flows, *Computer Methods in Applied Mechanics and Engineering*, 3, 269 – 289.

Ricardo, 2005: VECTIS Computational Fluid Dynamics (Release 3.9) user manual, Ricardo Consulting Engineers Ltd., Shoreham-by-Sea, UK, 578 pp.

Smith, S. D. 1980: Wind stress and heat flux over the Ocean in gale force winds', *J. of Phys. Ocean.*, **10**, 709-726.

Yelland, M. J., B. I. Moat, P. K. Taylor, R. W. Pascal, J. Hutchings and V. C. Cornell, 1998: Wind stress measurements from the open ocean corrected for airflow distortion by the ship, *Journal of Physical Oceanography*, **28**(7), 1511-1526.

Yelland, M. J., B. I. Moat, R. W. Pascal and D. I. Berry, 2002: CFD model estimates of the airflow over research ships and the impact on momentum flux measurements, *Journal of Atmospheric and Oceanic Technology,* **19**(10), 1477-1499.

Yelland, M. J., Pascal, R. W., Taylor, P. K. and Moat, B. I., 2009: AutoFlux: an Autonomous System for the Direct Measurement of the Air-Sea Fluxes of CO_2, Heat and Momentum, *Journal of Operational Oceanography, (in press)*

FIGURES

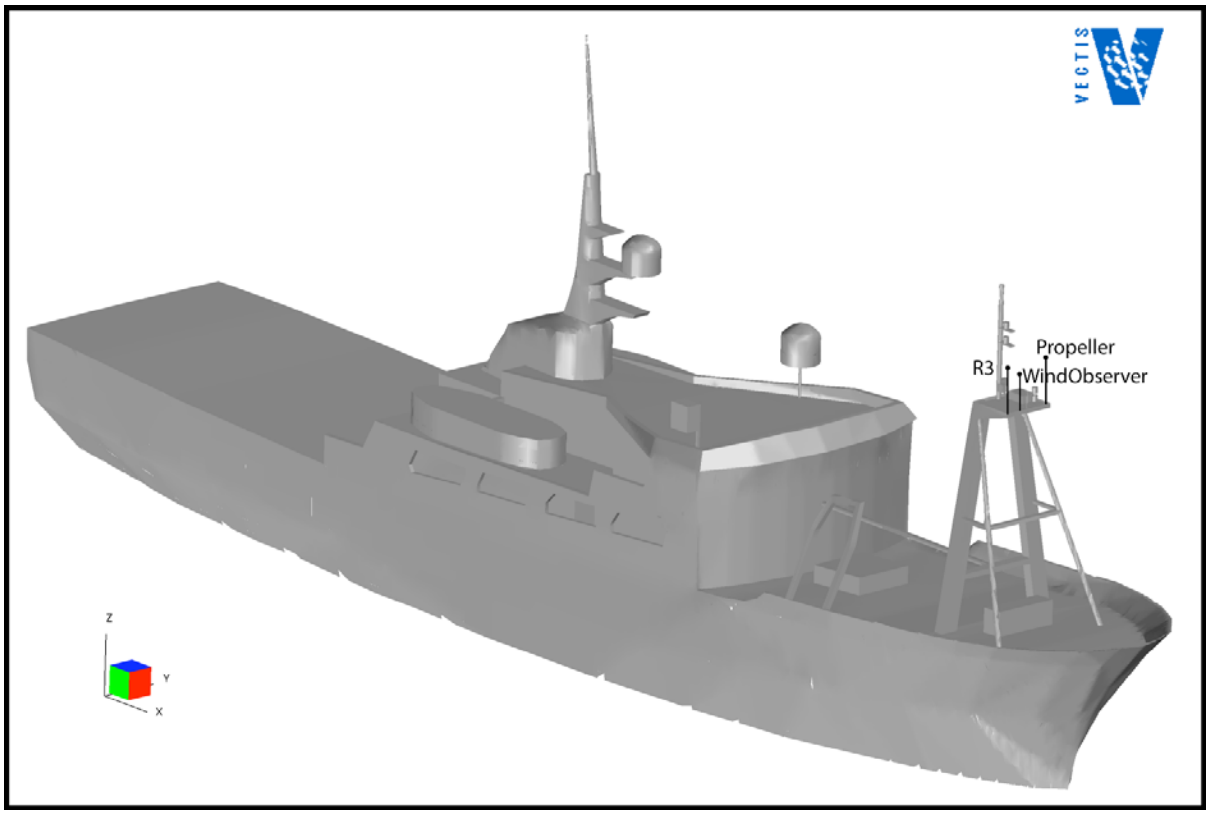

Figure 1 The *Polarfront* geometry. The NOCS R3 sonic anemometer, DNMI WindObserver and propeller anemometers are indicated.

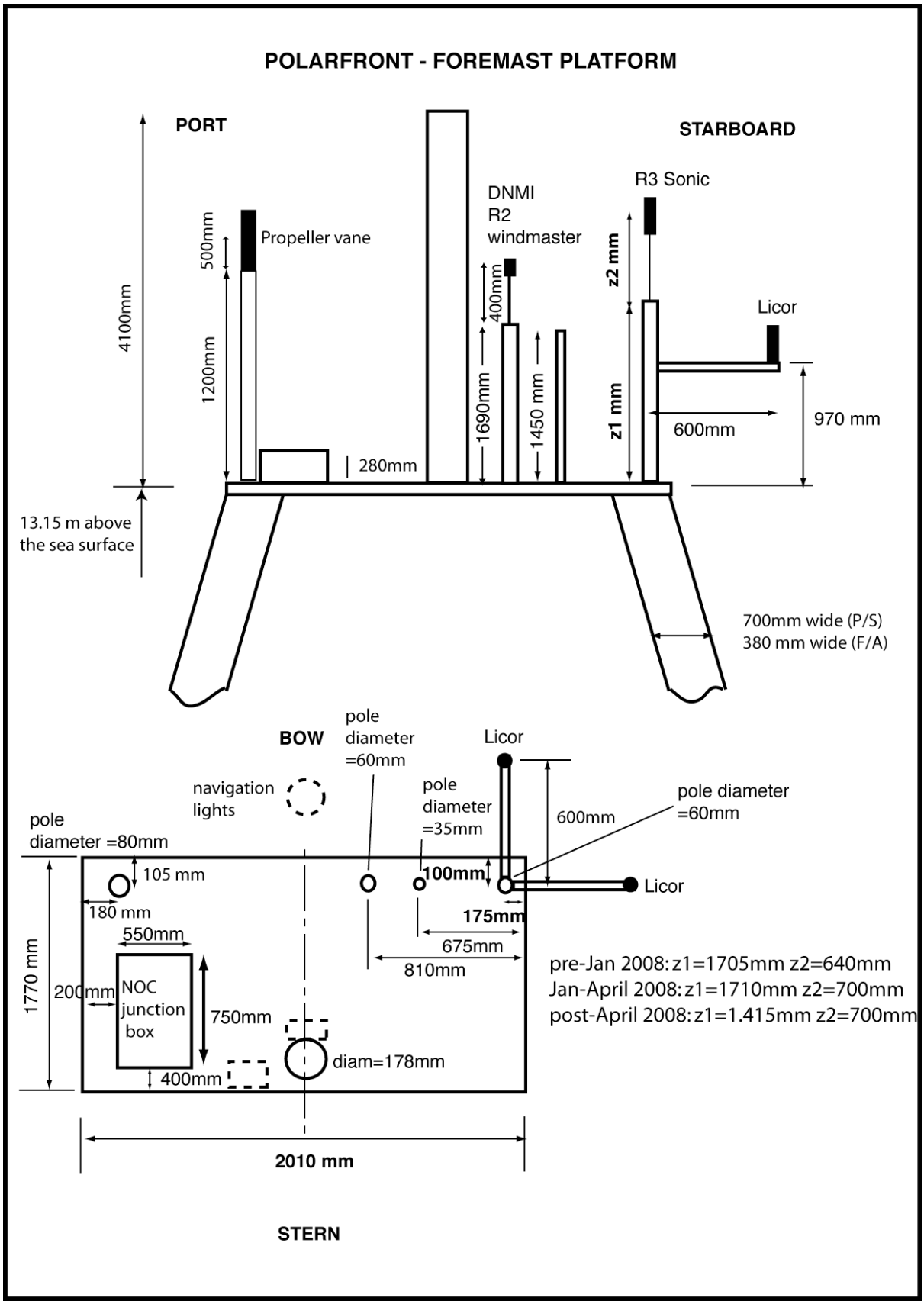

Figure 2 Schematic showing the instrument positions on the foremast.

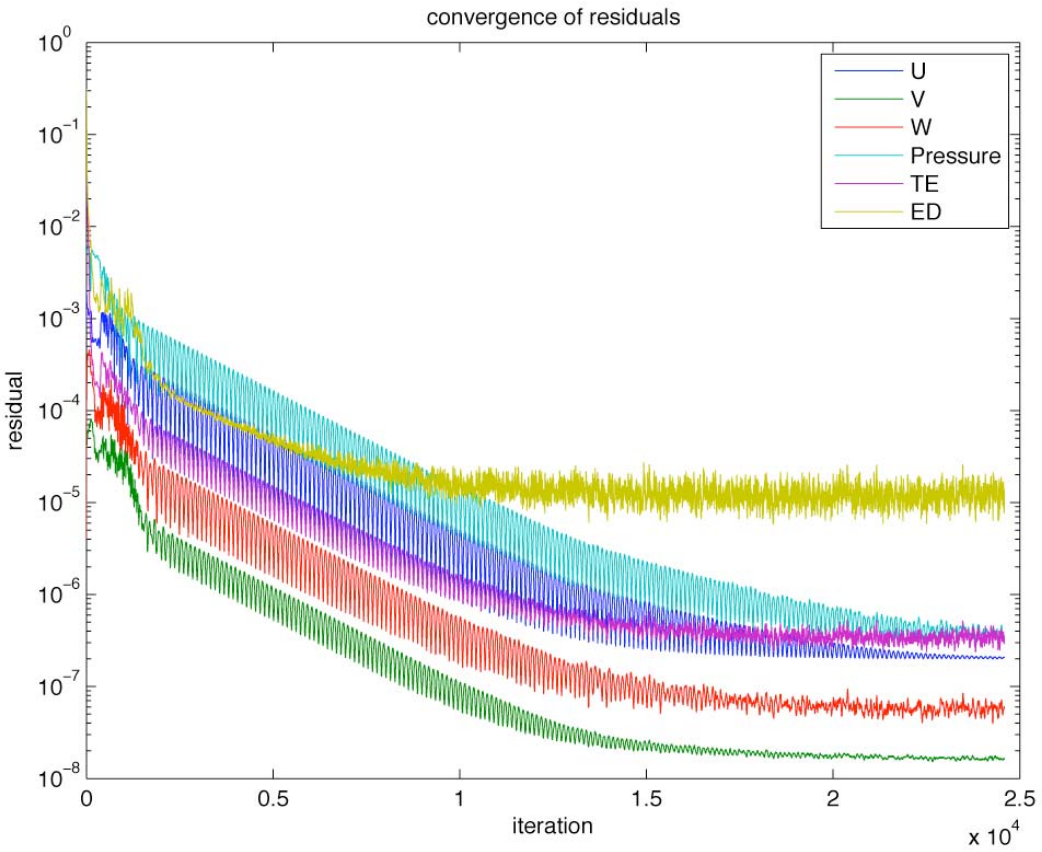

Figure 3 Convergence of the residuals (u, v, w velocity components; Pressure; TE turbulent kinetic energy and ED viscous dissipation) for the 0 degree simulation 3.10/4.

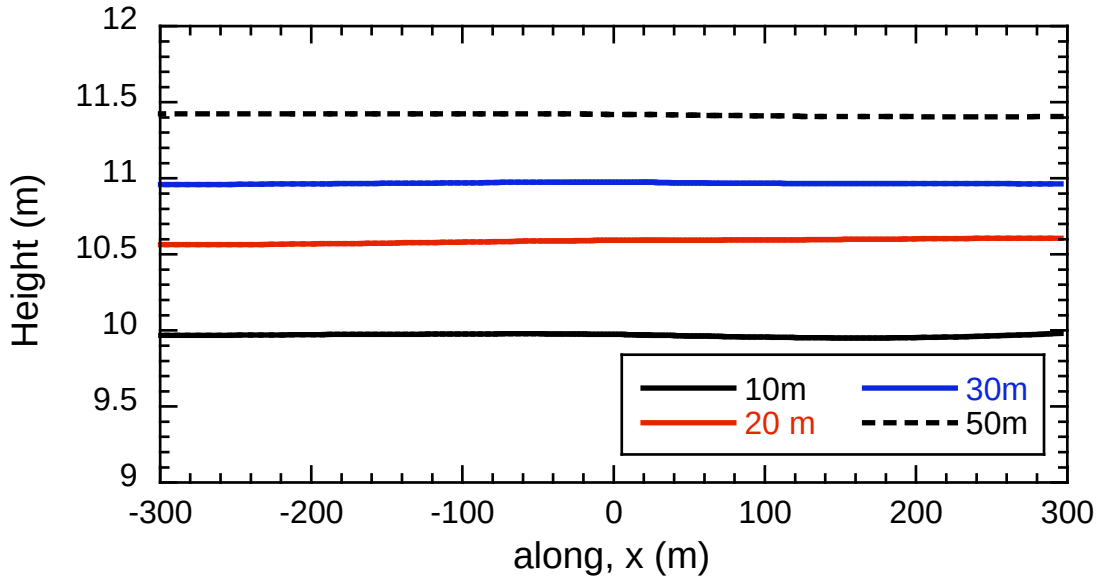

Figure 4 Lines of velocity data along the length of the tunnel at the heights shown. The data were obtained from the free stream region towards one side of the tunnel.

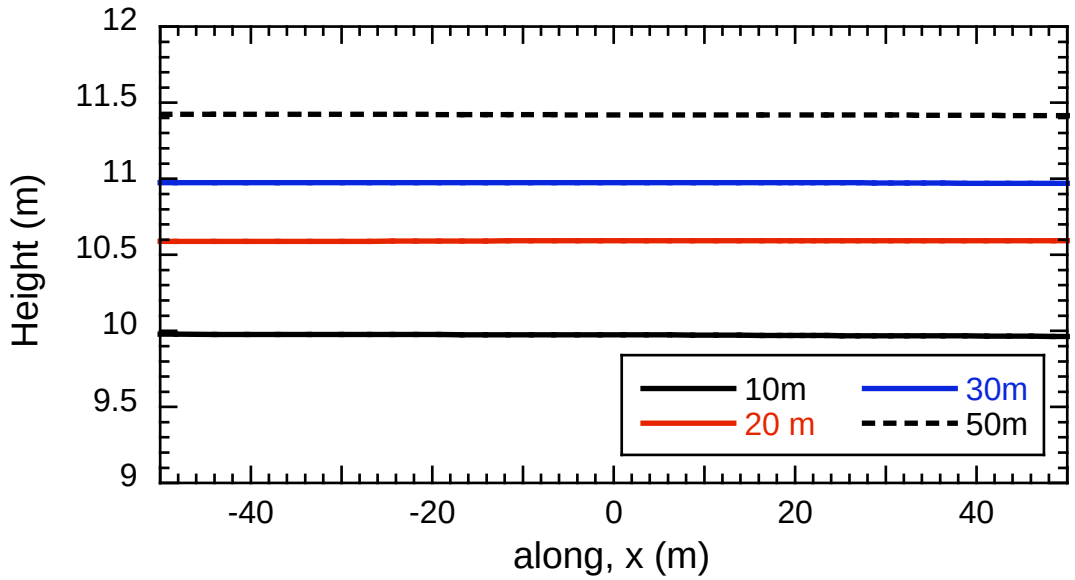

Figure 5 As Figure 4, showing the central portion of the tunnel only.

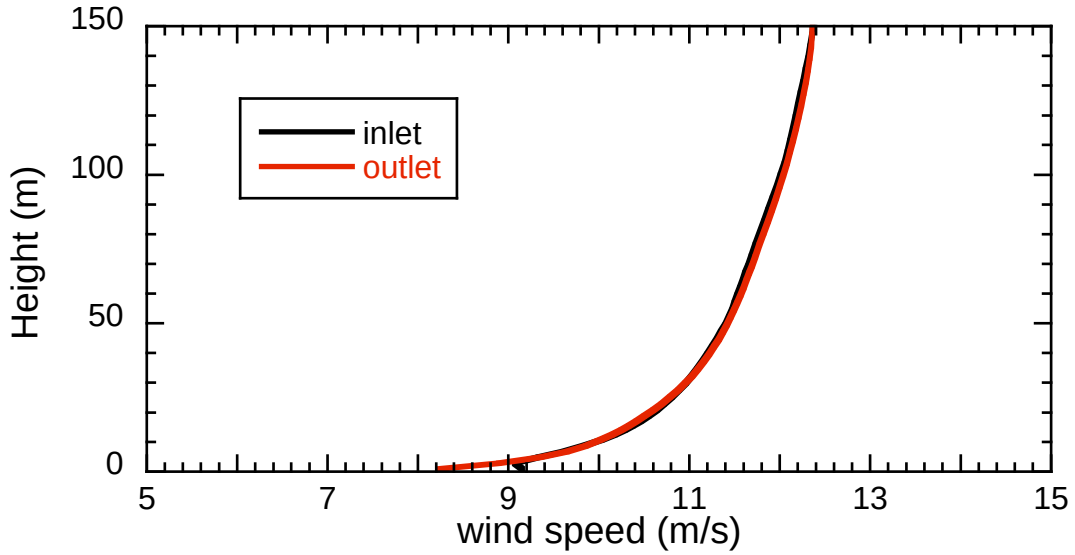

Figure 6. The vertical profiles of the velocity at the inlet (solid line) and outlet (dashed line) of the wind tunnel.

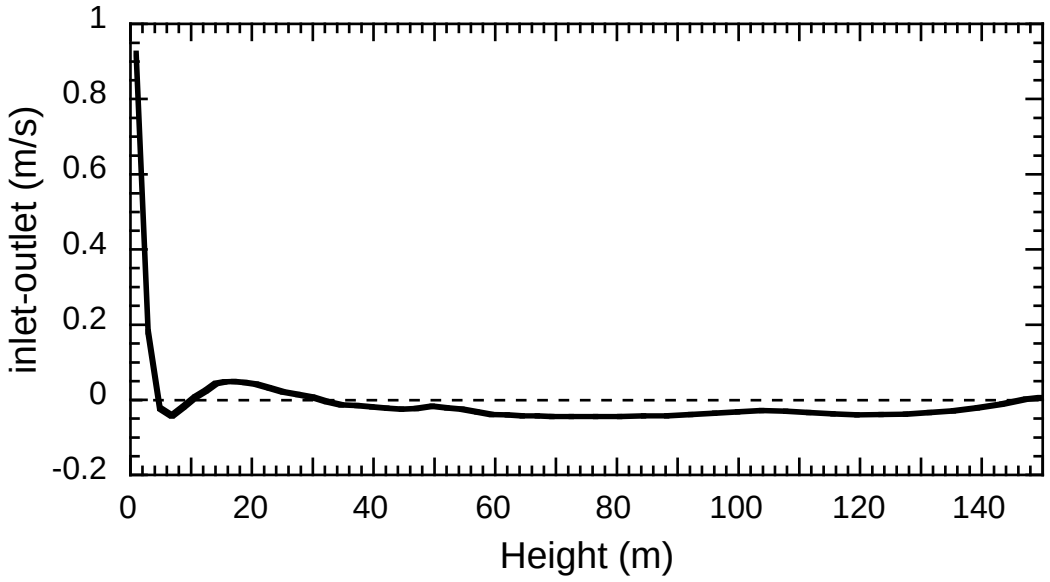

Figure 7 The difference between the vertical profiles of velocity shown in Figure 6.

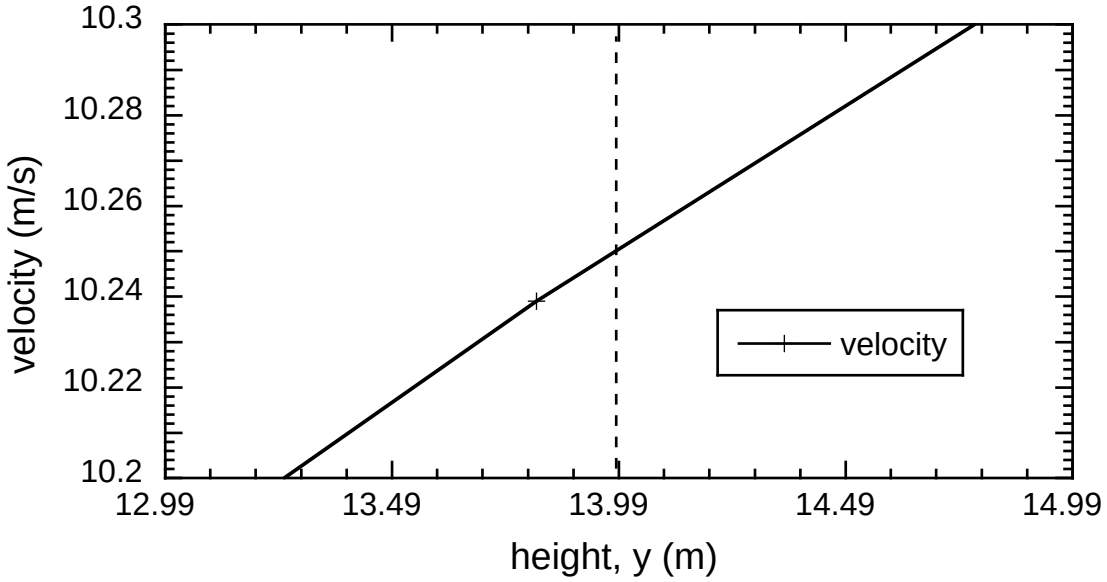

Figure 8 The vertical profile of velocity abeam of the foremast anemometer sites. The dashed line indicates the height from which the airflow to the R3 (post- April) originated.

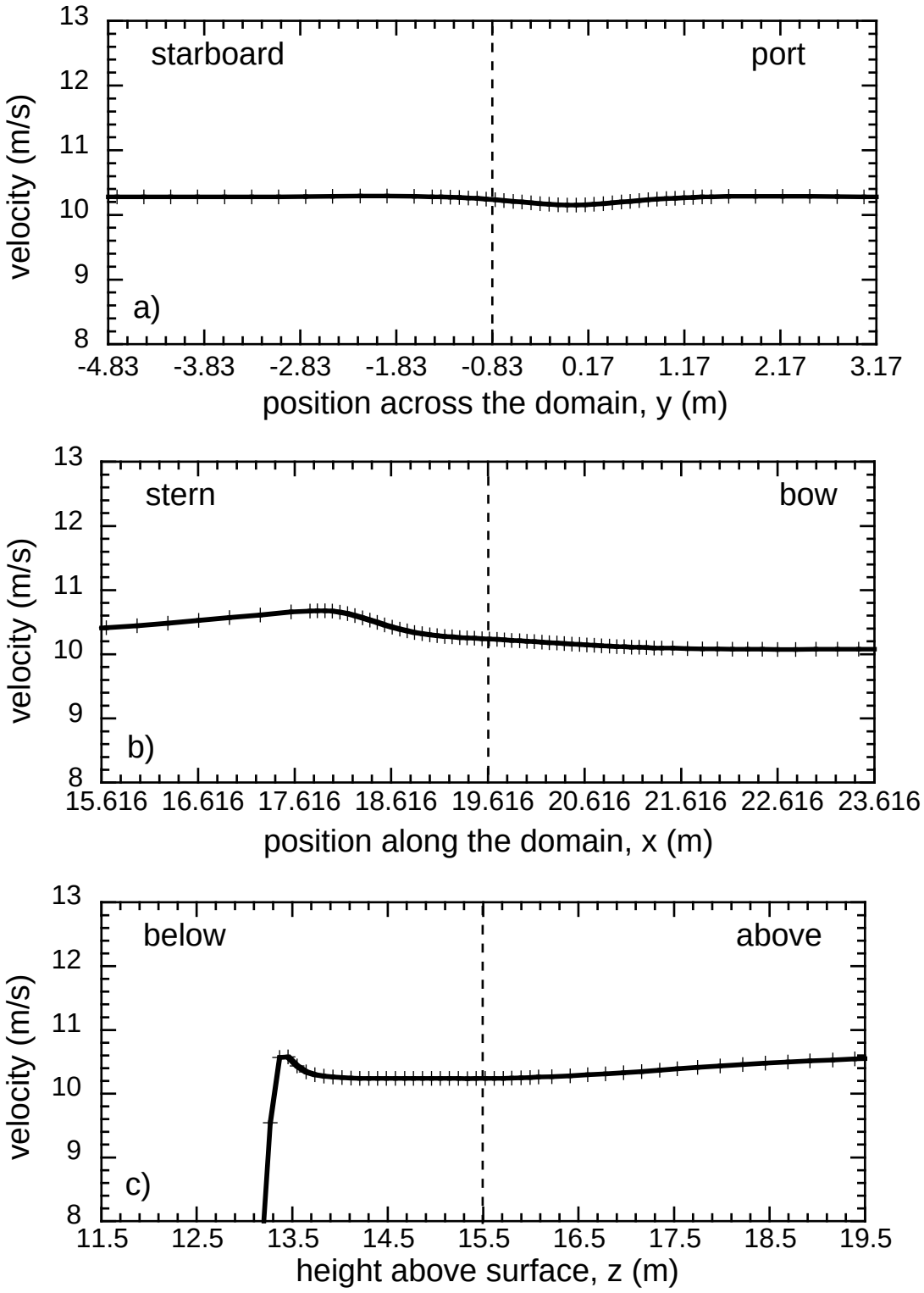

Figure 9 Lines of velocity data through the R3 (pre-January 2008) anemometer position (indicated by the dashed line) in all three directions; a) across the tunnel, b) along the tunnel, and c) vertically. Results are from a flow directly over the bow.

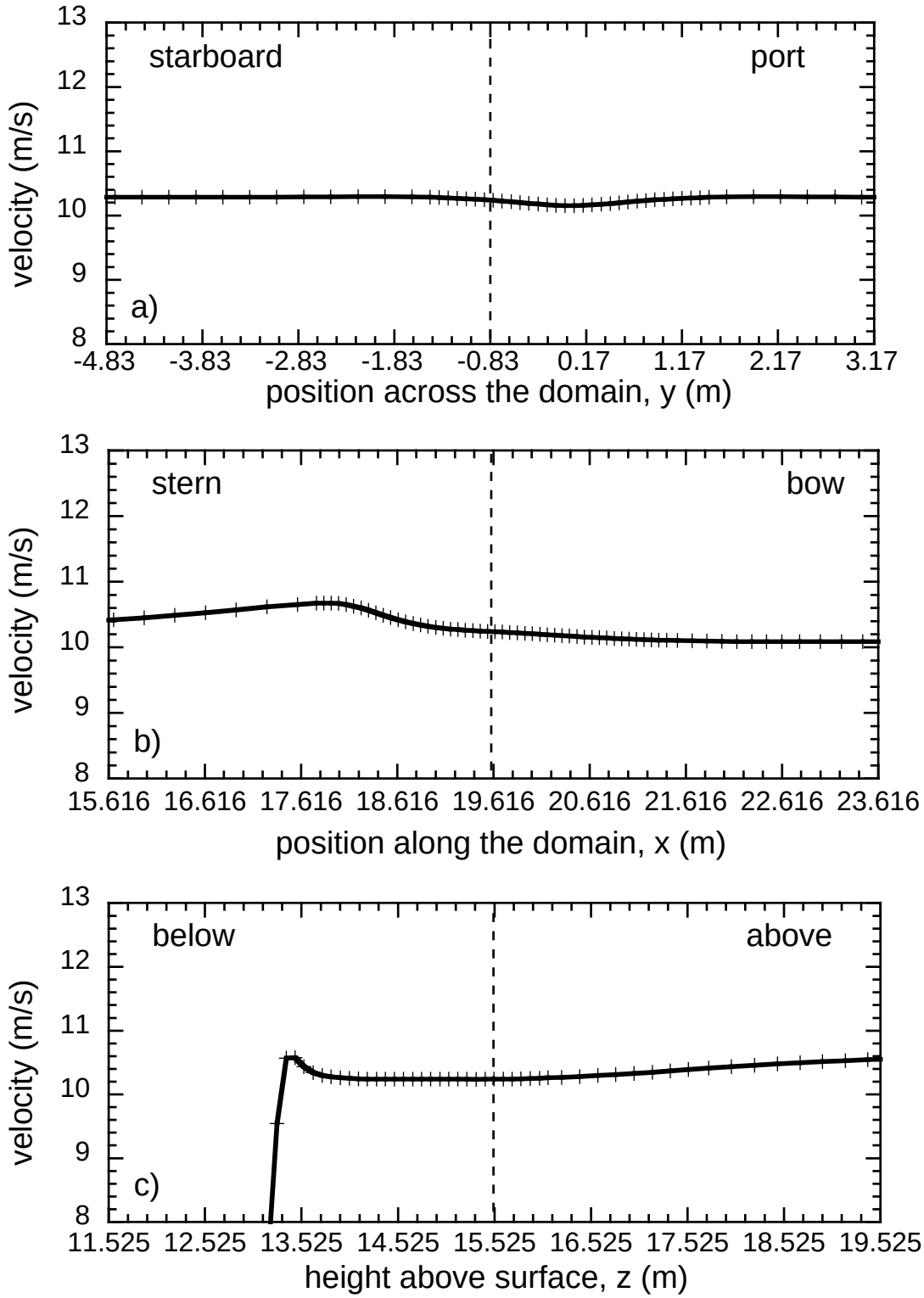

Figure 10 As Figure 9, but for the R3 anemometer site between January to April 2008. Results are from a flow directly over the bow.

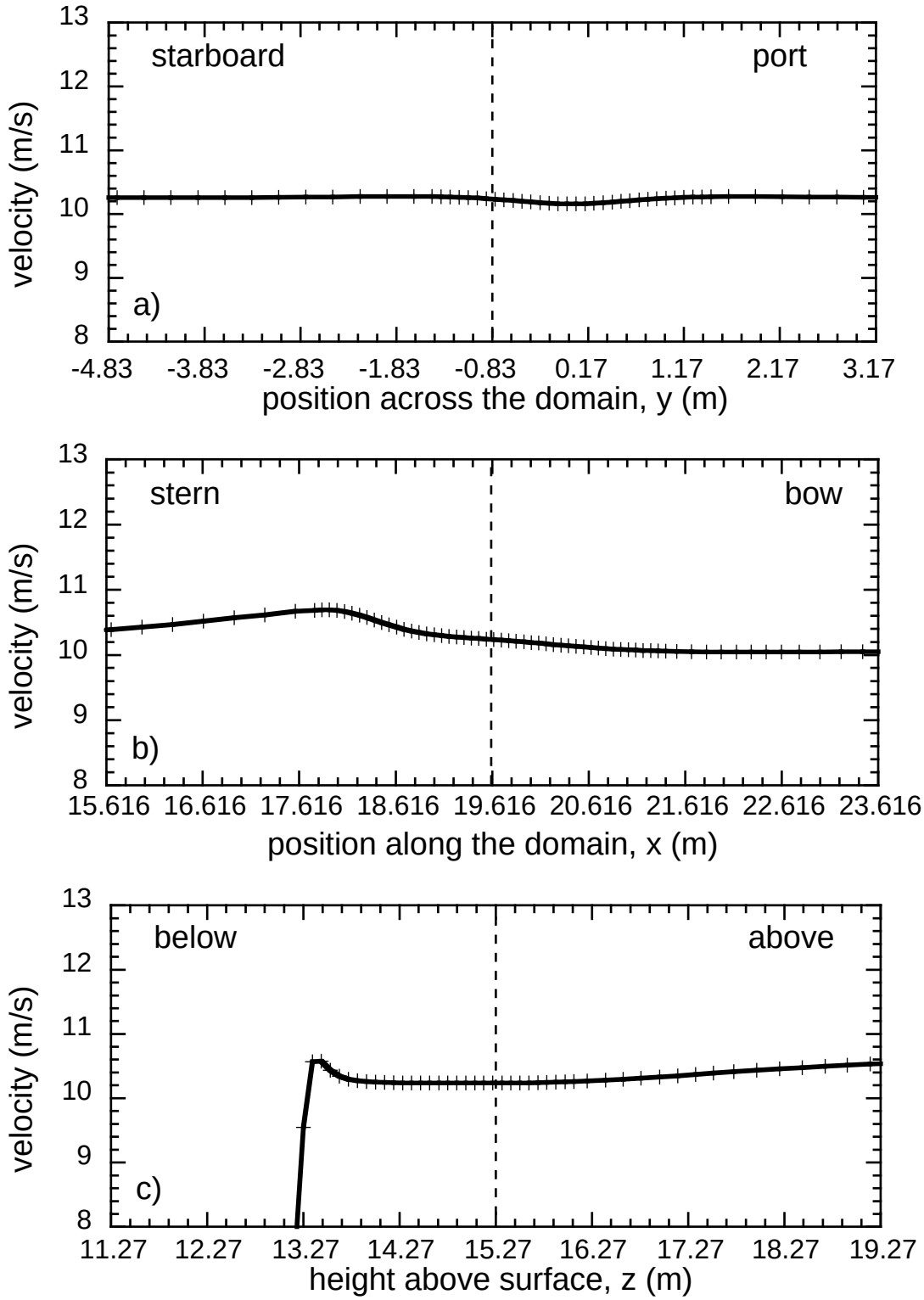

Figure 11 As Figure 9, but for the R3 anemometer post April 2008. Results are from a flow directly over the bow.

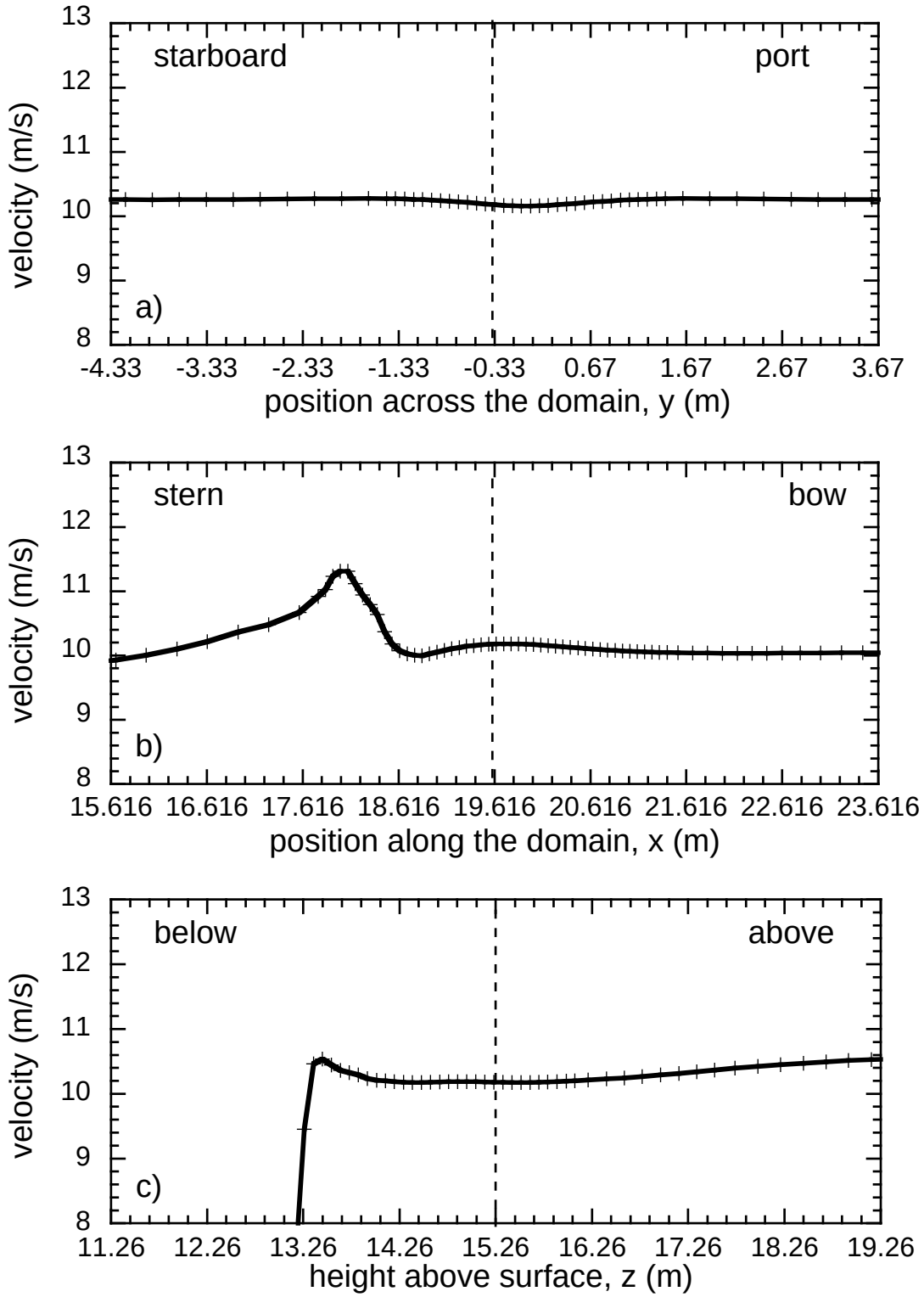

Figure 12 As Figure 9, but for the DNMI WindObserver anemometer. Results are from a flow directly over the bow.

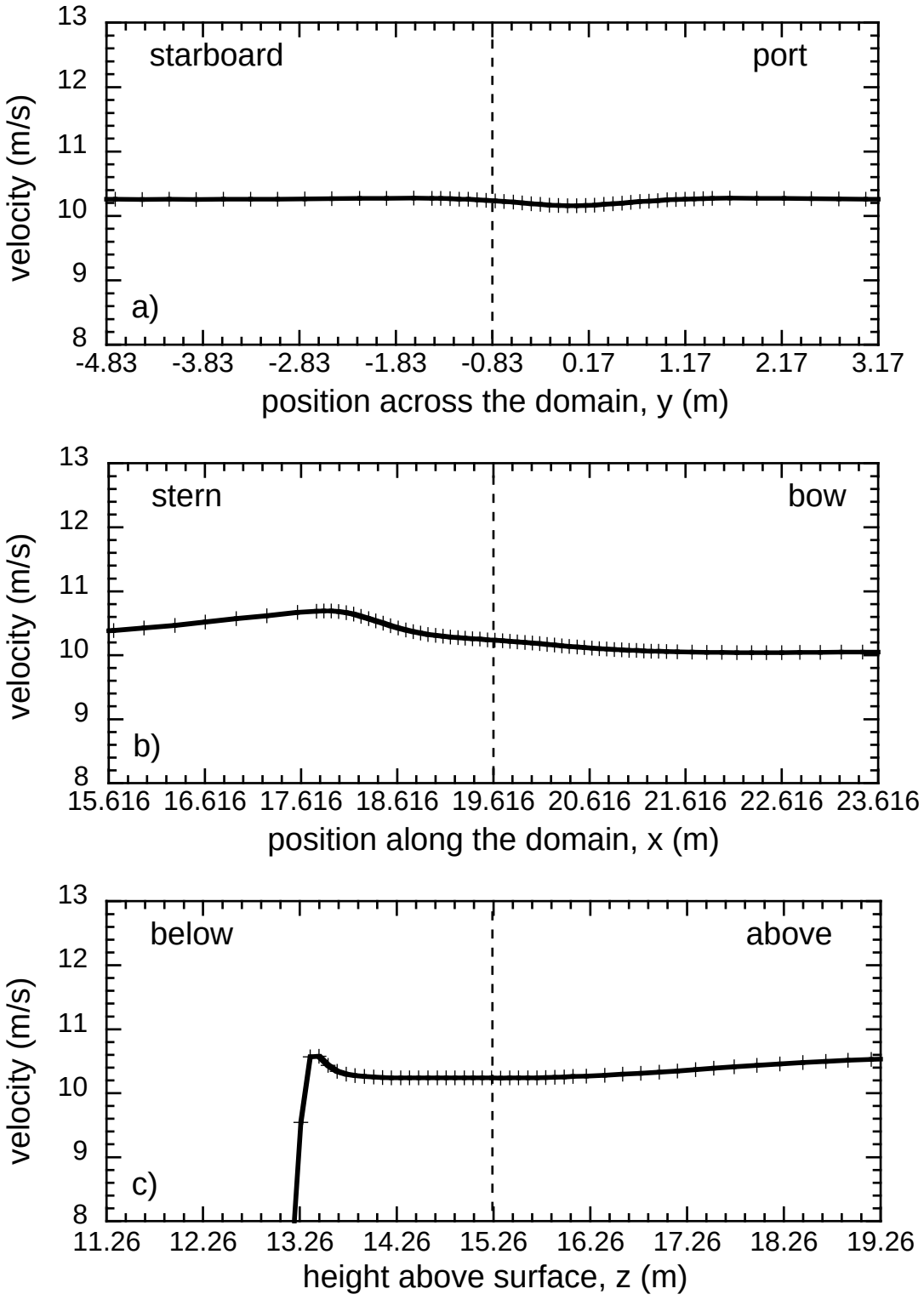

Figure 13 As Figure 9, but for the DNMI WindObserver anemometer pre-September 2008. Results are from a flow directly over the bow.

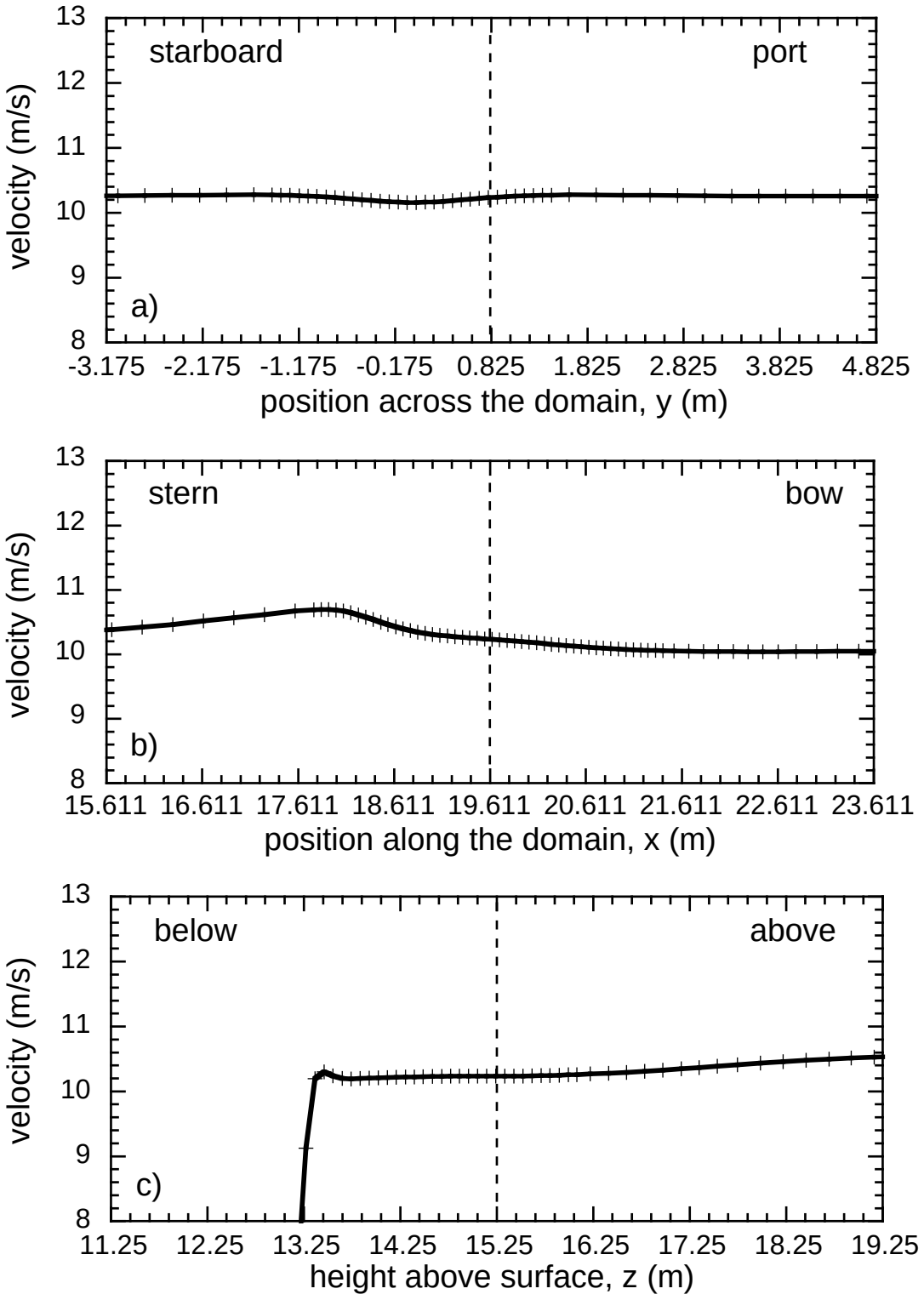

Figure 14 As Figure 9, but for the DNMI propeller anemometer. Results are from a flow directly over the bow.

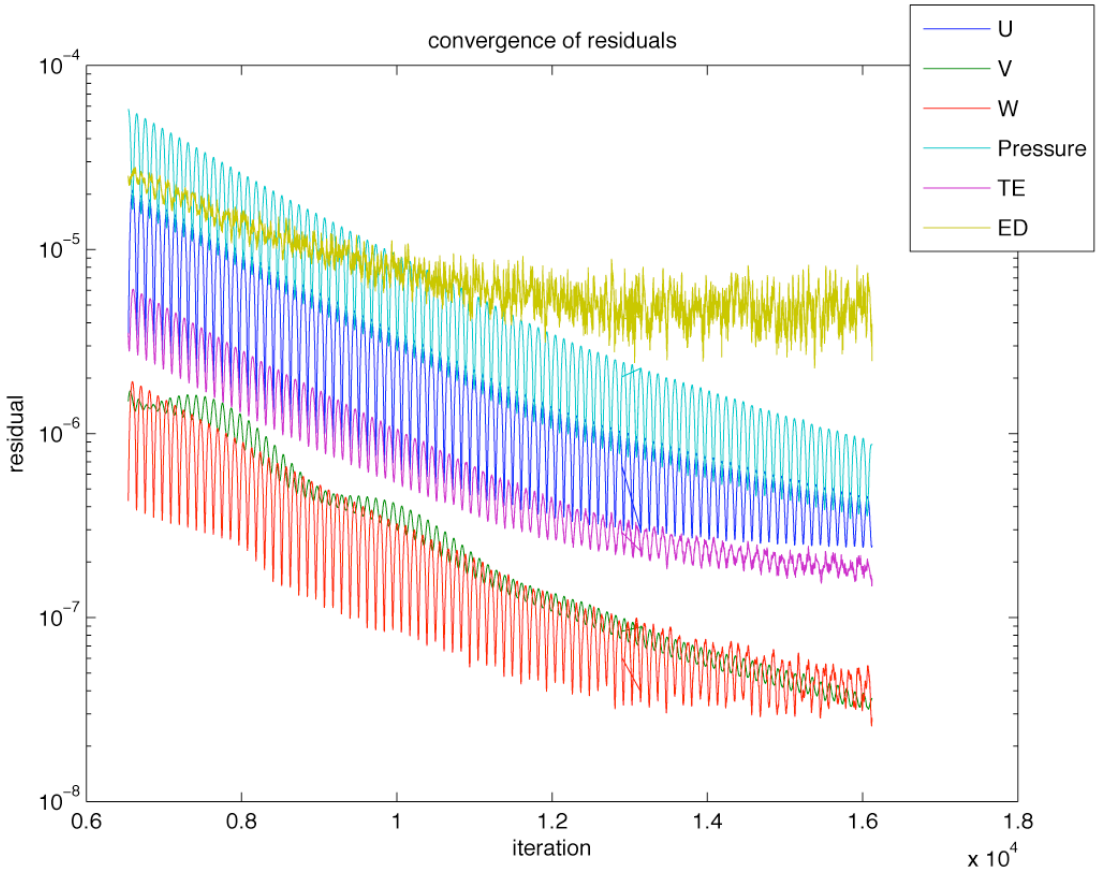

Figure 15 Convergence of the residuals (u, v, w velocity components; Pressure; TE turbulent kinetic energy and ED viscous dissipation) for the 100 degree airflow simulation 3.10/3.

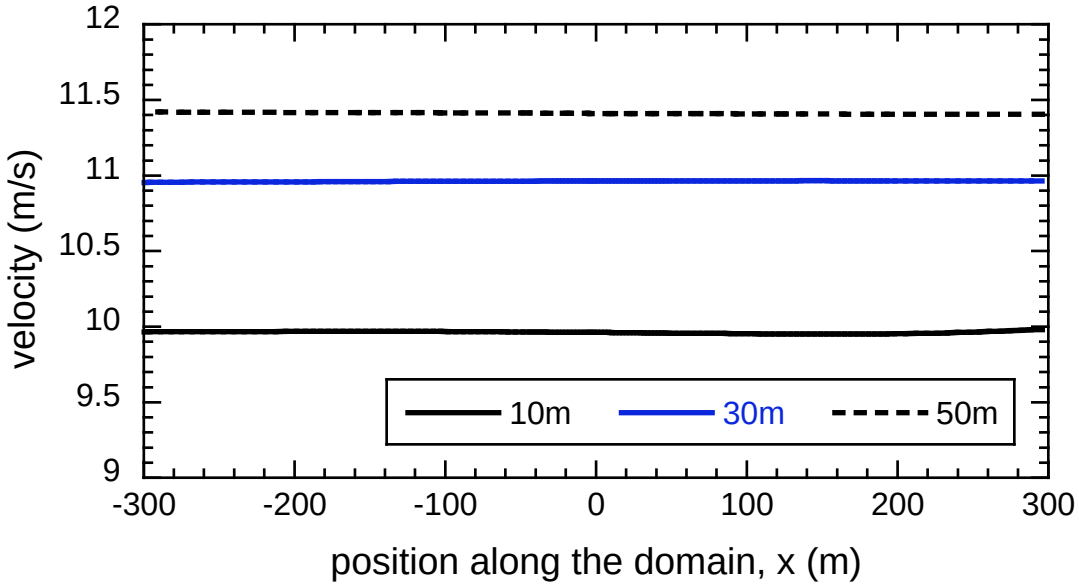

Figure 16 Lines of velocity data along the length of the tunnel at the heights shown. The data were obtained from the free stream region towards one side of the tunnel.

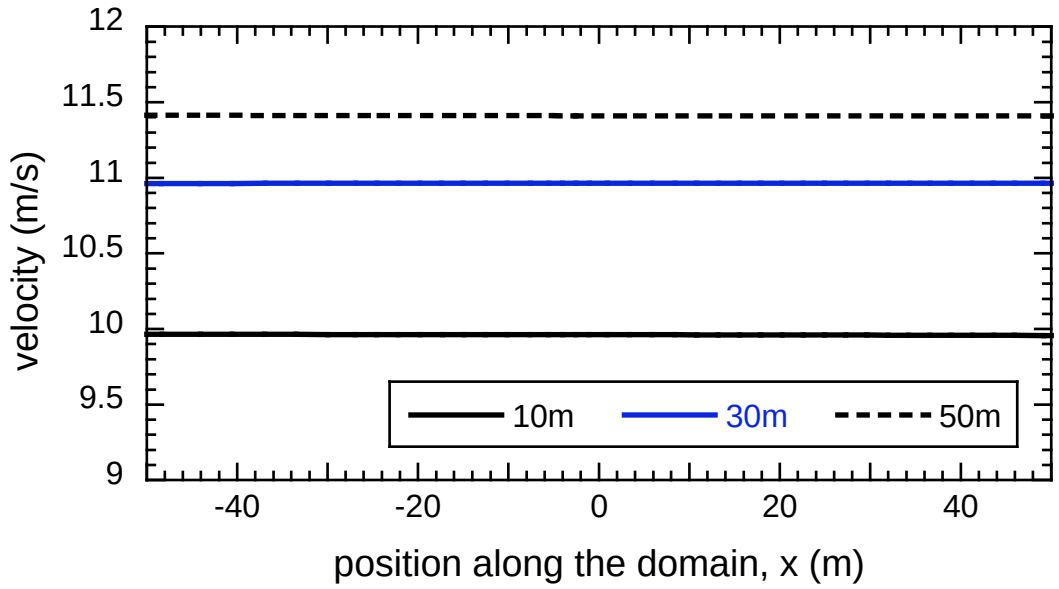

Figure 17 As Figure 16, showing the central portion of the tunnel only.

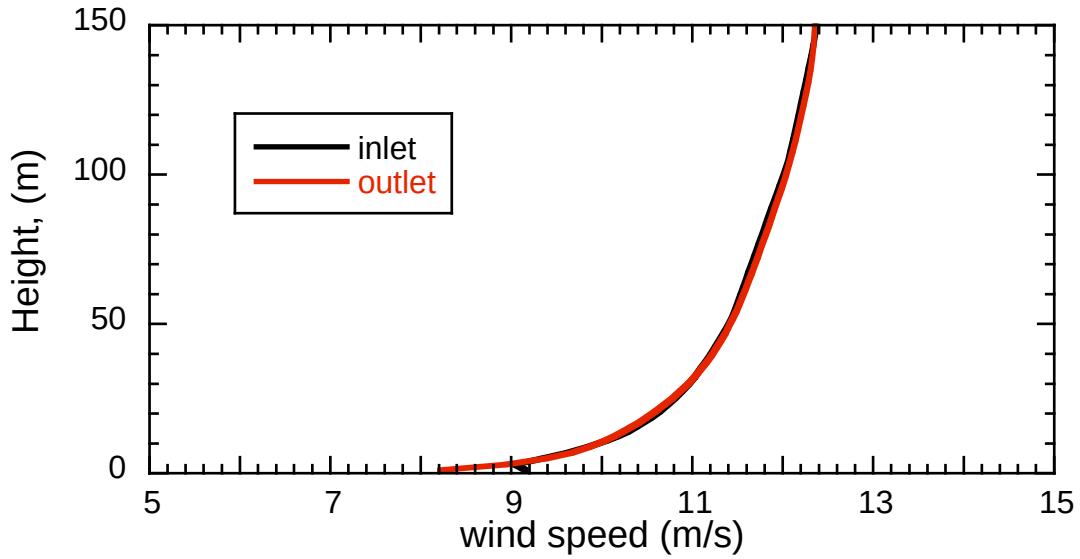

Figure 18 The vertical profiles of the velocity at the inlet (solid line) and outlet (dashed line) of the wind tunnel.

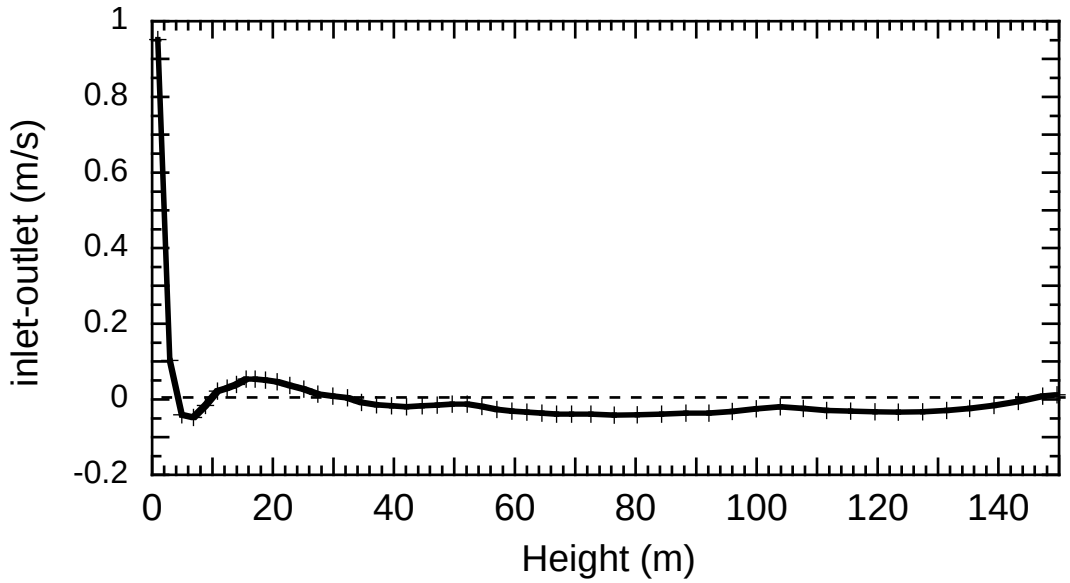

Figure 19 The difference between the vertical profiles of velocity shown in Figure 18.

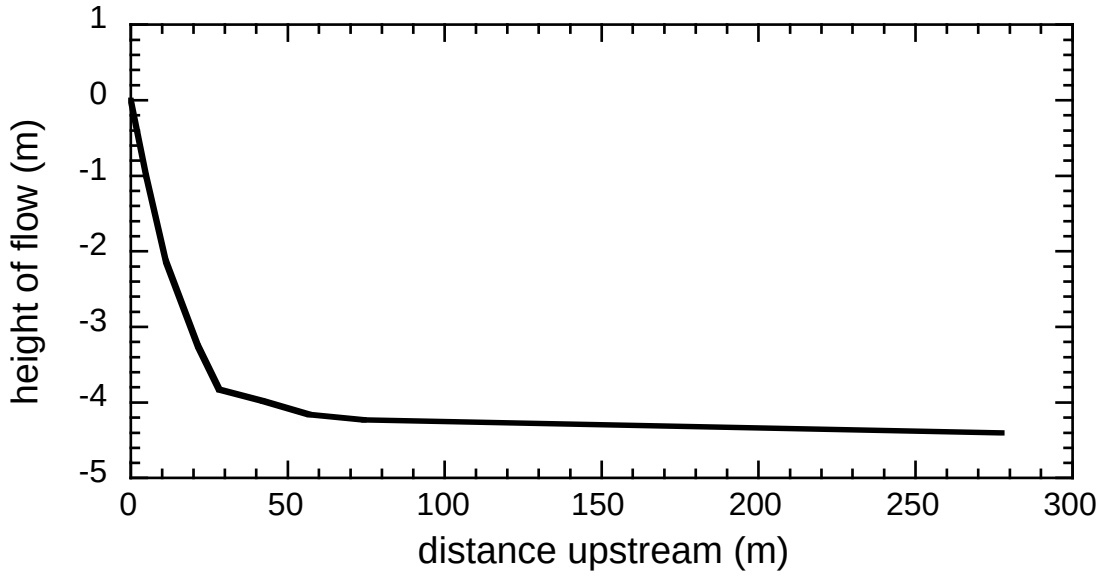

Figure 20 The variation of the vertical displacement of the flow with distance upwind of the anemometer. Results are from a flow 100° off the starboard bow.

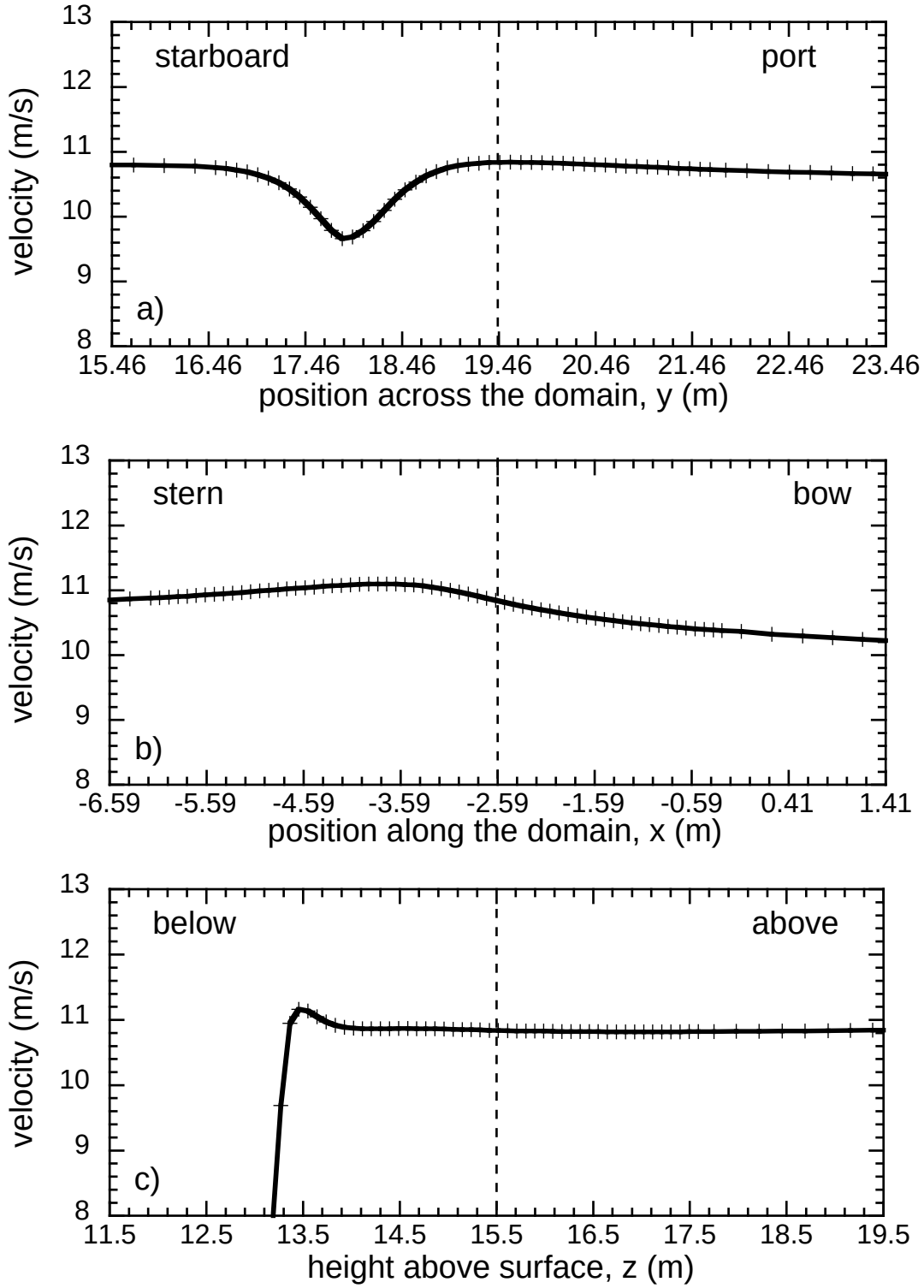

Figure 21 Lines of velocity data through the R3 (pre-January 2008) anemometer position (indicated by the dashed line) in all three directions; a) across the tunnel, b) along the tunnel, and c) vertically. Results are from a flow 100° off the starboard bow.

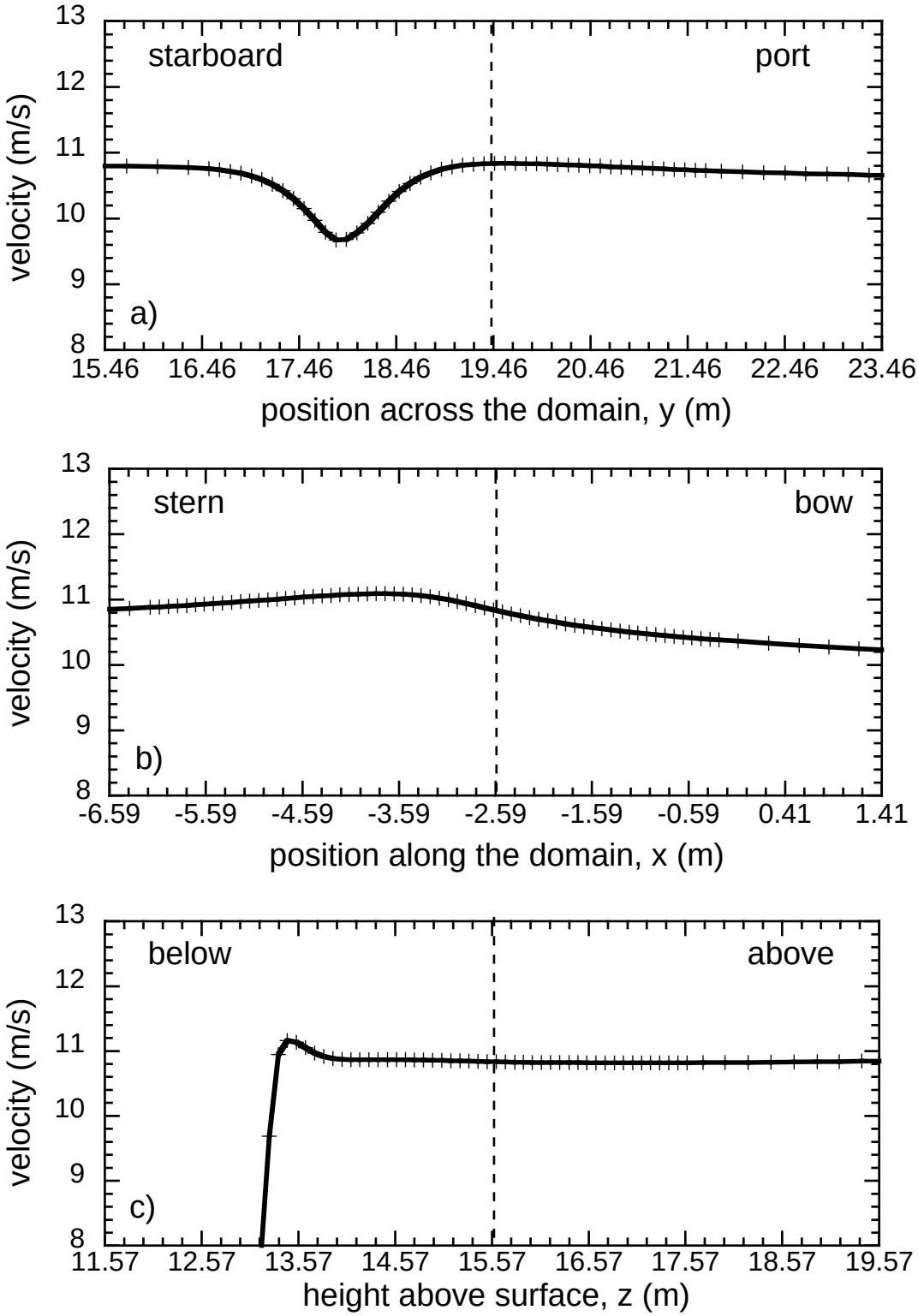

Figure 22 As Figure 21, but for the R3 anemometer site between January to April 2008. Results are from a flow 100° off the starboard bow.

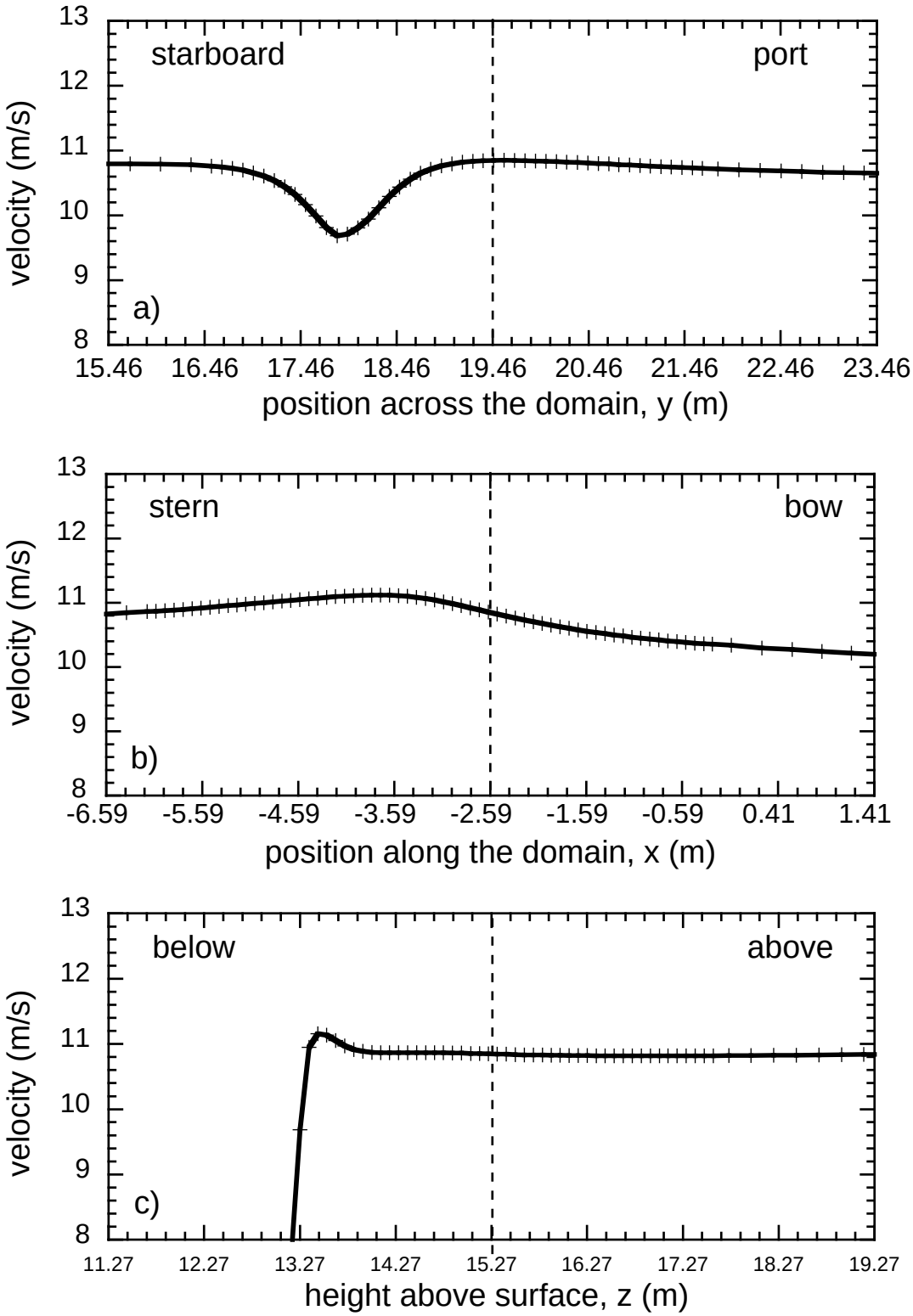

Figure 23 As Figure 21, but for the R3 anemometer post April 2008. Results are from a flow 100° off the starboard bow.

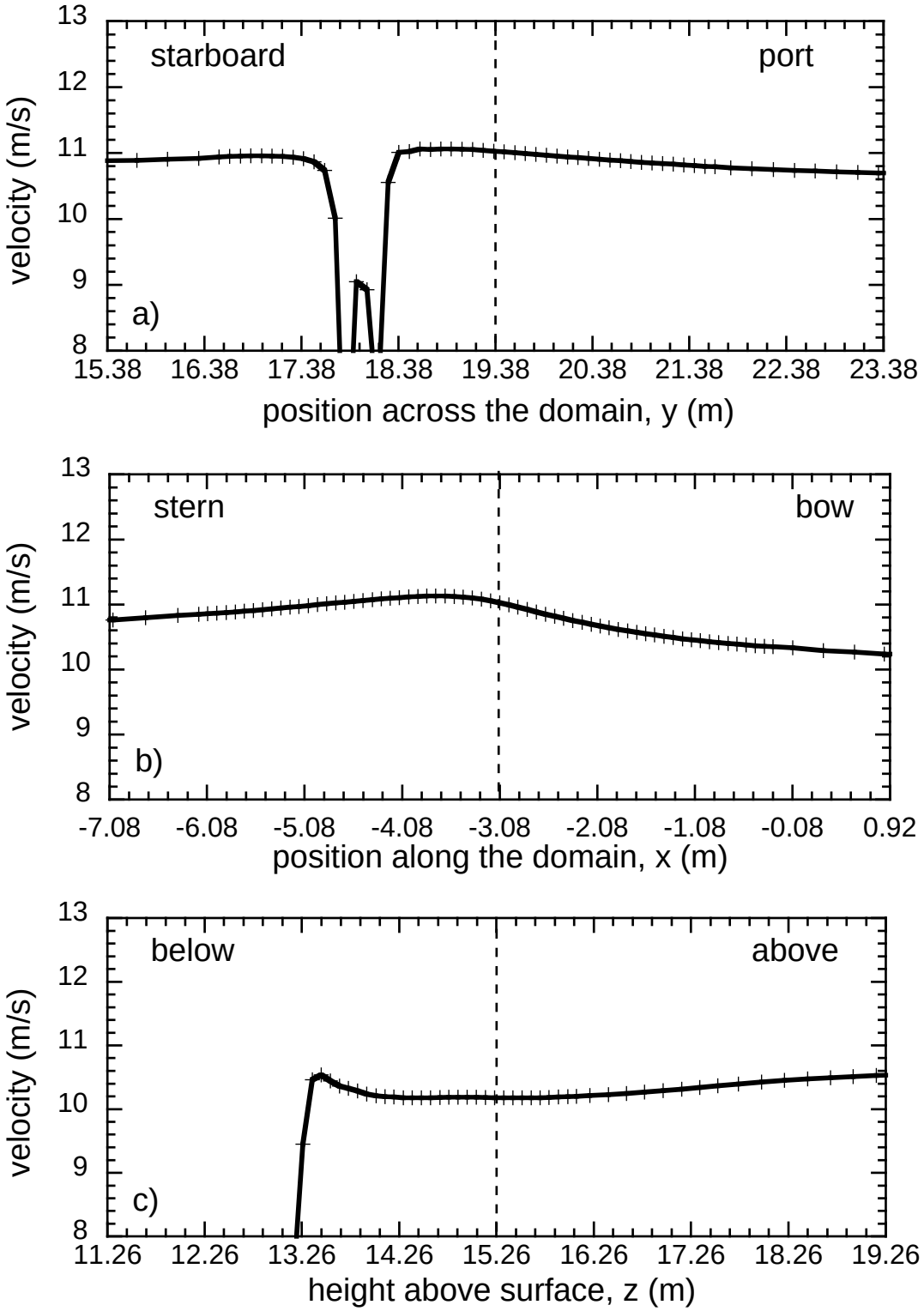

Figure 24 As Figure 21, but for the DNMI WindObserver anemometer. Results are from a flow 100° off the starboard bow.

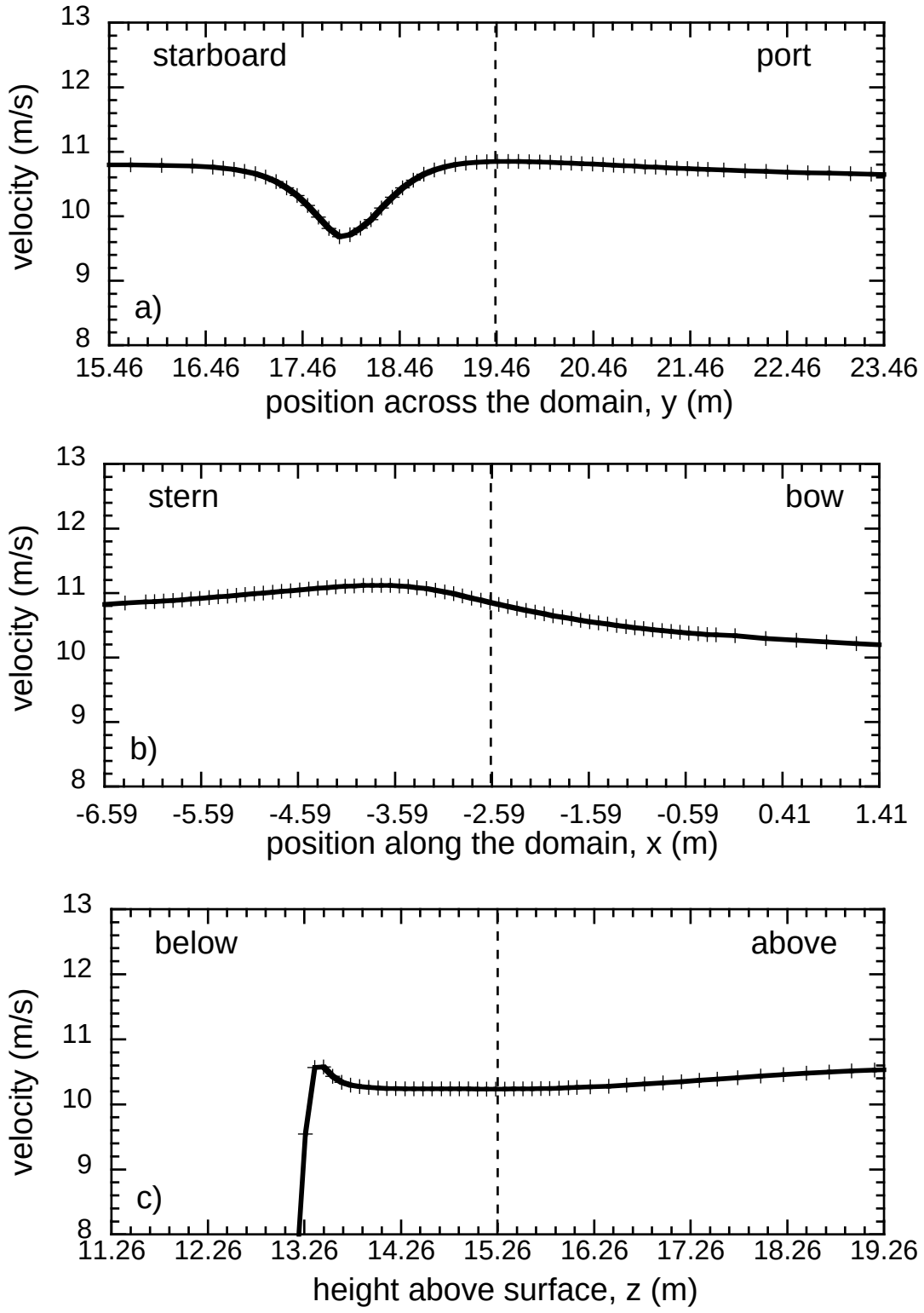

Figure 25 As Figure21, but for the DNMI WindObserver anemometer pre-September 2008. Results are from a flow 100° off the starboard bow.

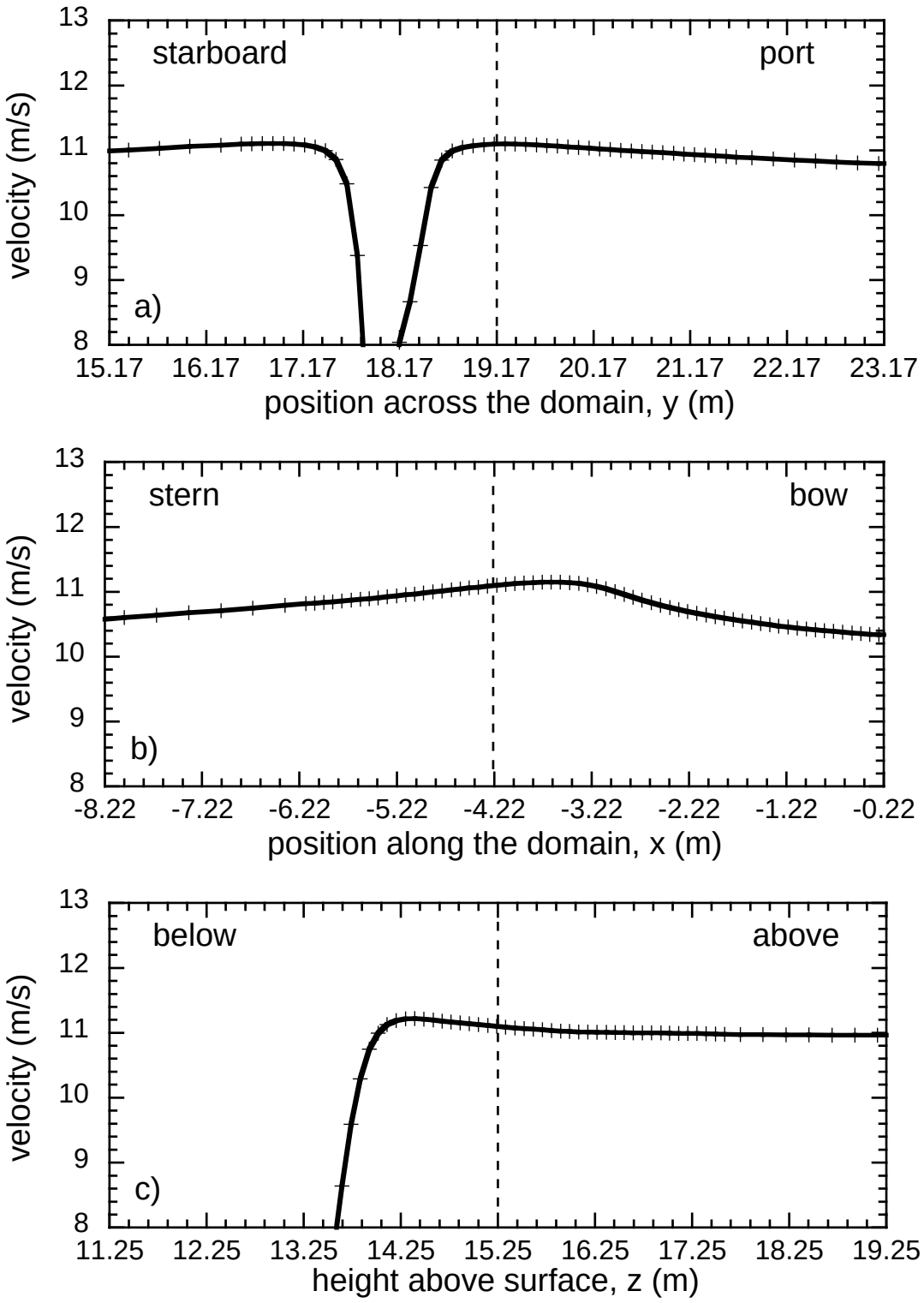

Figure 26 As Figure 21, but for the DNMI propeller anemometer. Results are from a flow 100° off the starboard bow.